Study of High-Energy Gamma-Ray Imaging Detectors for Fast Neutron Analysis

by

Gongyin Chen

B. Eng. in Engineering Physics, Tsinghua University, 1991

Submitted to the Department of Nuclear Engineering

in Partial Fulfillment of the Requirements for the Degree of

MASTER OF SCIENCE IN NUCLEAR ENGINEERING

AT THE

MASSACHUSETTS INSTITUTE OF TECHNOLOGY

June 1999

Signature of Author _____

Department of Nuclear Engineering

May 11, 1999

Certified by _____

Dr. Richard C. Lanza

Department of Nuclear Engineering

Thesis Advisor

Certified by _____

Professor Lawrence M. Lidsky

Department of Nuclear Engineering

Thesis Reader

Accepted by _____

Professor Lawrence M. Lidsky

Chairman, Department Committee on Graduate Students

Study of High-Energy Gamma-Ray Imaging Detectors for Fast Neutron Analysis

by

Gongyin Chen

Submitted to the Department of Nuclear Engineering

on May 11, 1999, in partial fulfillment of the requirements for the degree of

Master of Science in Nuclear Engineering

Abstract

Explosives and drugs have distinctive Carbon, Hydrogen, Oxygen, and Nitrogen contents. In this thesis, we introduce the Fast Neutron Analysis (FNA) technique for explosive and drug inspection. Fast neutrons induce gamma rays (mainly by inelastic scattering) of different energy from different nuclei and the intensity of a certain energy gamma ray represents the intensity of a corresponding nucleus. By imaging the induced gamma rays of different energies by Coded Aperture Imaging (CAI) method, we obtain a mapping of elemental distribution and are therefore able to recognize hidden explosives and drugs.

The processes of Neutron penetration and gamma ray production are studied using MCNP-4A code and Coded Aperture Imaging method is briefly introduced. The results have shown that FNA technique when combined with CAI method offers a solution in elemental mapping, and therefore explosive and drug inspection.

Great emphasis is given in the detector performance. Energy resolution, spatial resolution, and detection efficiency have been studied in detail. A sodium iodide (NaI) array detector and a bismuth germanate (BGO) bar detector are proposed for use in CAFNA or as a prototype. Monte Carlo simulation shows that the two detector choices fulfill the requirements of CAFNA.

Thesis Supervisor: Richard C. Lanza

Title: Senior Research Scientist, Department of Nuclear Engineering

Acknowledgements

I would like to thank my thesis advisor, Dr. Richard Lanza, for his guidance and assistance during the past year. His dedication, patience, humor, and more importantly, physics insight have been very helpful to me and are greatly appreciated.

I am very grateful to have such great colleague and friend, Roberto Accorsi, as my fellow graduate student. I also thank Prof. Richard Freifelder and prof. Joel S. Karp of Department of Radiology, University of Pennsylvania, and Prof. Jeffery Schweitzer of Physics Department, University of Connecticut, for the valuable discussions with them.

I would like to thank Prof. Lawrence M. Lidsky for serving as my thesis reader.

Table of Contents

List of Figures

List of Tables

Chapter 1 Introduction

Illegal drugs and the possibility of terrorists using explosives are two of the biggest problems the United States faces [1]. Different types of methods have been proposed and tried to detect such kinds of goods [1][2], some widely used. Among them, nuclear techniques have unique advantages in that they are non-invasive and they perform real time inspection, therefore allowing the inspection of a large flow of objects. In this thesis, Fast Neutron Analysis technique is proposed for both drug and explosive detection and high-energy gamma ray detectors have been designed for the purpose of Coded Aperture Imaging. This technique may also be used for general elemental imaging and the detectors may be used in telescopes in gamma ray astronomy.

1.1 Background and Problems

Explosives transported onto airplanes by terrorists greatly threaten the lives of passengers and jeopardize the aviation industry. Illegal drugs from the Southwest border spread all over the country. Great efforts have been made to fight against those crimes, in airports, passenger luggage is screened, mostly for weapons including explosives. On the border, cargo containers and trucks or cars are inspected, for drugs (and other goods as well).

Among the existing methods, X-ray planar radiography is the most widely used one in airport security check. Medium energy X-rays (~140kev) go through the inspected object and are partly absorbed, giving information about the attenuation coefficient (and therefore substance density, given the X-ray energy range) integrated along its path. A similar technique is used in cargo container inspection, where higher energy X-rays or gamma rays are used.

Drugs and explosives, however, have densities close to ordinary goods. It is difficult to identify such kinds of contraband simply by density difference. Fortunately, drugs and explosives have unique elemental composition. Composition of general drugs and explosives are given in table 1.1. (Data from [1].)

Table 1.1 Elemental Density (g/cm^3) of Contraband and Common Materials

	Material	Hydrogen	Carbon	Nitrogen	Oxygen
1	NITROGLY	0.0352	0.2544	0.2960	1.0144
2	EGDN	0.0355	0.3256	0.2531	0.8658
3	AMNIT	0.0850	0.0000	0.5950	0.9860
4	BLPOWDER	0.0000	0.4026	0.1830	0.6588
5	NCEL	0.0384	0.3888	0.2256	0.9472
6	PETN	0.0422	0.3344	0.3115	1.0683
7	DETASHEET	0.0636	0.4647	0.1806	0.7711
8	TNT	0.0359	0.6031	0.3016	0.6895
9	COMP-B	0.0462	0.4172	0.5216	0.7302
10	PBSTY	0.0211	0.4651	0.2718	0.9302
11	TETRYL	0.0299	0.4864	0.4050	0.7404
12	DYN	0.0500	0.1750	0.2188	0.7375
13	HMX	0.0532	0.3078	0.7182	0.8208
14	C3	0.0464	0.3648	0.5248	0.6656
15	C4	0.0594	0.3614	0.5693	0.6633
16	PICRIC	0.0229	0.5526	0.3221	0.8606
17	PBAZ	0.0000	0.0000	1.2947	0.0000
18	TRIAC	0.1164	0.4644	0.0000	0.6192
19	HEXA	0.0906	0.5432	0.2120	0.7253
20	WOOL	0.0071	0.0563	0.0329	0.0377
21	SILK	0.0080	0.0593	0.0432	0.0395
22	DACR	0.0063	0.0938	0.0000	0.0500
23	ORLON	0.0086	0.1019	0.0396	0.0000
24	NYLON	0.1106	0.7262	0.1414	0.1619
25	POLYES	0.0056	0.1001	0.0000	0.0444
26	COTTON	0.0090	0.0720	0.0000	0.0690
27	RAYON	0.0093	0.0660	0.0000	0.0740
28	POLYET	0.1344	0.8056	0.0000	0.0000
29	POLYPR	0.1316	0.7884	0.0000	0.0000
30	PVC	0.0638	0.5107	0.0000	0.0000
31	SARAN	0.0419	0.4050	0.0000	0.0000
32	LUCITE	0.1056	0.6334	0.0000	0.4222
33	NEOPR	0.0550	0.8000	0.0000	0.0000
34	PAPER	0.0434	0.3080	0.0000	0.3451
35	ALCOH	0.1048	0.4168	0.0000	0.2720
36	SUGAR	0.1040	0.6720	0.0000	0.8240
37	OIL	0.0960	0.6160	0.0000	0.0880
38	BARLEY	0.0685	0.4320	0.0100	0.4700
39	SOYBE	0.0750	0.4900	0.844	0.3510
40	WOOD	0.0441	0.3808	0.0000	0.2744
41	WATER	0.1110	0.0000	0.0000	0.8890
42	POLYUP	0.0869	0.5775	0.3058	0.1342
43	MELAM	0.0768	0.4576	1.0656	0.0000
44	HERION	0.0628	0.6820	0.0379	0.2166
45	HHCL	0.0569	0.6214	0.0345	0.1971
46	COCAI	0.0692	0.6730	0.0461	0.2110
47	COCL	0.0653	0.6003	0.0412	0.1883
48	MORPH	0.0067	0.7156	0.0491	0.1682
49	PCP	0.0104	0.8587	0.0576	0.0000
50	LSD	0.0078	0.7427	0.1299	0.0495

Characteristics of our interest are summarized in table 1.2. Some drugs are rich in Chlorine when they are in large amount. (as for example cocaine Hydrochloride) It is clear that an elemental mapping is sufficient to identify drugs and explosives.

Table 1.2: Characteristics of drugs and explosives

	Rich in	Poor in	Ratio	Density
Drugs	C, H, Cl	N, O	High C/O	-
Explosives	N, O	C, H	Low C/O	High N, O
Common Goods	H, C, N	O	-	Low N

Fast Neutron Analysis (FNA) technique introduces a fast neutron beam into interested object and detects the secondary gamma rays from neutron interactions. Here the object irradiated by neutron beam is a multi-energy radiation source (analogous to color)—different elements give rise to gamma rays of different energy upon interaction with neutron. When combined with Coded Aperture Imaging (CAI) technique, it is possible to obtain the spatial distribution of different elements.

1.2 Thesis Outline

This thesis consists of seven chapters. Chapter 1 (this chapter) introduces the background and the thesis structure. Chapter 2 discusses the Fast Neutron Analysis method. After an overview of nuclear medicine, fast neutron penetration and gamma-ray production are studied. Monte Carlo Simulation results are given. Chapter 3 briefly introduces Coded Aperture Imaging. General designs and performance are discussed. Chapter 4 summarizes the requirements of the imaging detector to be used. NaI(Tl) and BGO detectors are chosen for further analysis. Chapter 5 studies the performance of a NaI(Tl) crystal detector. Transport of scintillation light is simulated and different installations are compared and performance is predicted. Chapter 6 gives another choice of detector—BGO. Light transport is again studied to give energy and spatial resolution information.

Chapter 7 summarized the results and conclusions we obtain so far. Future development is also suggested. The appendices contain some of the computer codes used in our study.

Chapter 2 Fast Neutron Analysis (FNA)

2.1 Neutron Activation Analysis

There is a similarity between industrial applications and medical applications [8] of radiation. Fast Neutron Analysis is the counterpart of injecting radioactive matter into human body and imaging its distribution.

2.1.1 Overview of Nuclear Medicine and X-ray techniques

Nuclear Techniques are widely used in nuclear medicine. X-ray planar radiography and X-ray computer tomography give maps of X-ray attenuation coefficient, which to a large extent depends on the chemical composition and physical state (density) of the human tissues. These methods therefore provide only morphological information.

On the other hand, when radioactivity is introduced into human body, mostly by injection or digestion, the images show the perfusion or the subsequent concentration of radioactive substance in the human body. These images show physiological function directly, which is far more useful in the early diagnosis of disease. Various nuclear medicine methods are discussed in detail by Barrett [8].

2.1.2 Limitation of X-ray Systems

X-ray radiography and Computer Tomography are the most commonly used method without internal source. They both use an external radiation source at one side of object and a detector at the other side. The detector array (or screen) records the transmitted X-ray, which interacts with matter via [12]:

(a) Photoelectric Interaction

The incident X-ray (photon) vanishes, knocking an electron out from the atom.

(b) Compton Scattering

The incident photon knocks an electron out from the atom and its own energy is significantly reduced. Compton scattering dominants in the medium energy range.

(c) Pair Production.

When the incident photon energy is above 1.022Mev, it may vanish (in the existence of a nucleus), giving rise to an electron-positron pair.

The transmission of X-ray may be modeled as

$$I=I_0*e^{(-\mu.t)}$$

In the energy range from 100kev to 2-3Mev, compton scattering dominants. The attenuation coefficient (μ) is proportional to electron density, and therefore physical density (roughly speaking). The imaging recorded on the detector is a map of density integrated along the path of X-ray. X-ray Computer Tomography is similar, except that it uses the data of views from different angles and a reconstruction algorithm to obtain the 3-D density mapping.

2.1.3 Interactions of Neutrons with Matter

Most elements interact with neutron and usually give rise to prompt gamma rays. Therefore, an object irradiated by neutrons is, in effect, a COLOR gamma ray source. Different elements give rise to gamma rays of different energies. Let us first study the interaction of neutrons with matter, in the view of our interest.

Fast neutrons interact with matter in several ways, broadly classified as follows [3]:

(a) Elastic Scattering

The neutron hits a target nucleus at rest, and transfers part of its kinetic energy to the nucleus, which undergoes no structural change. This is the dominant process of losing energy and slowing down.

(b) Inelastic Scattering

Some of the incident neutron energy imparted to the target nucleus excites it to higher-energy state. The excited state lasts for typically 1 nanoseconds or less, and the ensuring prompt return to ground state usually results in the emission of a gamma ray. Such an interaction involving carbon ^{12}C, for example, gives a gamma ray of energy 4.44Mev. The interaction is written as

$$^{12}C(n, n' \gamma)^{12}C$$

In inelastic scattering, the neutron continues on, but at reduced energy.

(c) Reaction

The target nucleus experiences a structural change and the incident neutron usually disappears. An important example is the neutron induced alpha emission from oxygen, which results in the production of a ^{13}C isotope and the annihilation of the neutron. The ^{13}C nucleus may be already at ground state, or it may be excited, in which case a gamma ray is promptly emitted. The process is denoted as:

$$^{16}O(n,\alpha)^{13}C \text{ or } ^{16}O(n, \alpha \gamma)^{13}C$$

(d) Activation

The target nucleus is transformed to an unstable intermediate isotope, which decays with a relatively long half-life to the final nucleus. If the daughter nucleus is in an excited state, a prompt emission of gamma radiation accompanies the return to ground state.

When neutron losses its energy, its gets THERMALIZED. Thermal neutron interacts with matter via capture, reaction and scatter.

(a) Capture

The neutron is absorbed, or captured. And the resulting nucleus (always at excited state) decays to ground state with the emission of a gamma ray, or even transforms to another nucleus.

(b) Scattering

In thermal neutron scattering, the only result is the re-distribution of kinetic energies between the neutron and the target nucleus. The neutron scatters till it is captured or decays to a proton.

(c) Reaction

The neutron vanishes, producing a new particle.

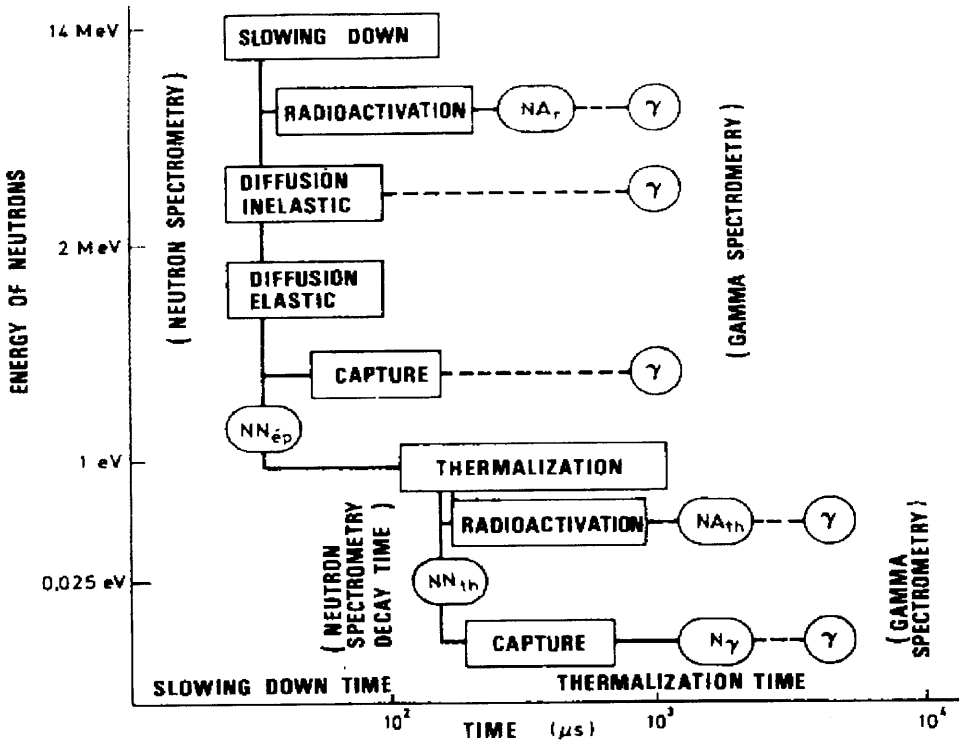

Figure 2.1 Neutron Interaction with matter

Figure 2.1 summarizes neutron interactions. Fast neutron inelastic scattering and reaction give rise to prompt gamma rays. Thermal neutron capture also gives prompt gamma ray. That is the foundation of Prompt Gamma Ray Neutron Activation Analysis.

Both fast neutron activation and thermal neutron capture may lead to long half-life nuclei. Detecting the residual radioactivity is another branch of neutron activation analysis, not of interest for this application.

2.2 Fast Neutron Analysis

Fast Neutron Analysis records the prompt gamma rays from fast neutron interactions. In addition, when the inspected object is large, fast neutron may eventually be thermalized. Thermal neutrons also induce prompt gamma rays in the capture process. Figure 2.2 illustrates Fast Neutron Analysis (Combined with Coded Aperture Imaging).

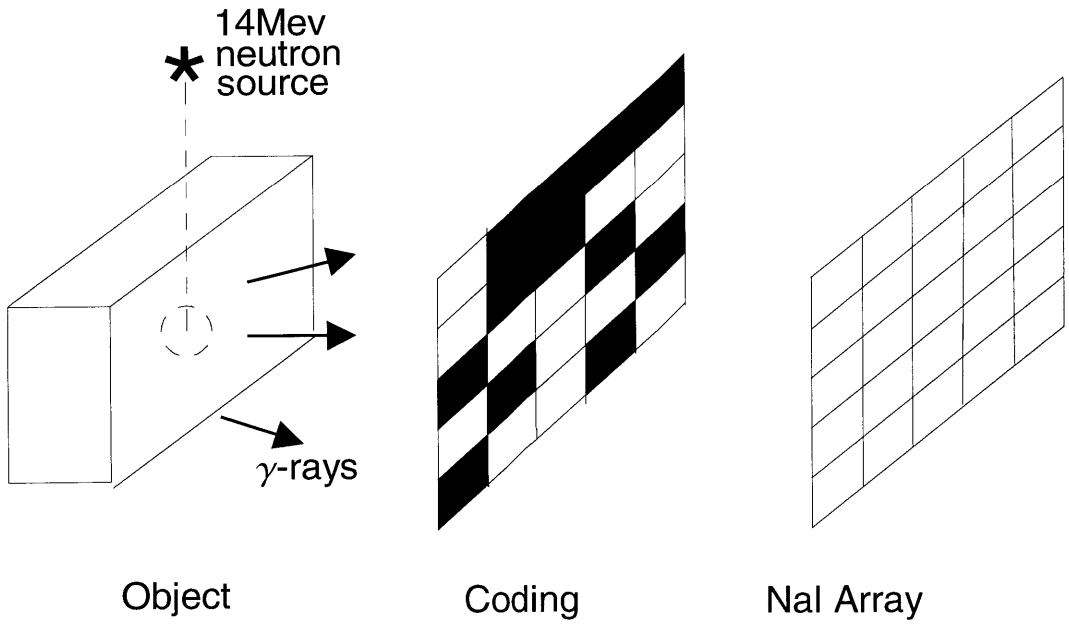

Figure 2.2 Principal of Fast Neutron Analysis (with CAI)

2.2.1 Neutron Interaction Cross-Sections

All types of neutron interactions contribute to the decrease in neutron flux. Certain types mentioned above lead to prompt gamma ray emission. Figure 2.3 gives cross section data for Carbon, Nitrogen, Oxygen and Hydrogen [3][7]. The resonance peaks usually corresponds to inelastic scattering or reaction, leading to the emission of prompt gamma rays. Also, thermal neutron induced gamma ray (capture gamma ray) may provide valuable information about elemental content. Indeed, it is the foundation of Thermal

Neutron Analysis or TNA. [3][4] Thermal Neutron cross sections for several nature elements are given in table 2.1. Capture is especially important for Chlorine.

Table 2.1 Thermal Neutron Cross Sections for Nature Elements (barns)

	Total	Capture (n, γ)	Reaction (n, p)
Hydrogen	20.81	0.33	-
Carbon	4.74	0.03	-
Nitrogen	11.80	0.08	1.85
Oxygen	3.89	0.00	-
Chlorine	49.70	32.85	0.36

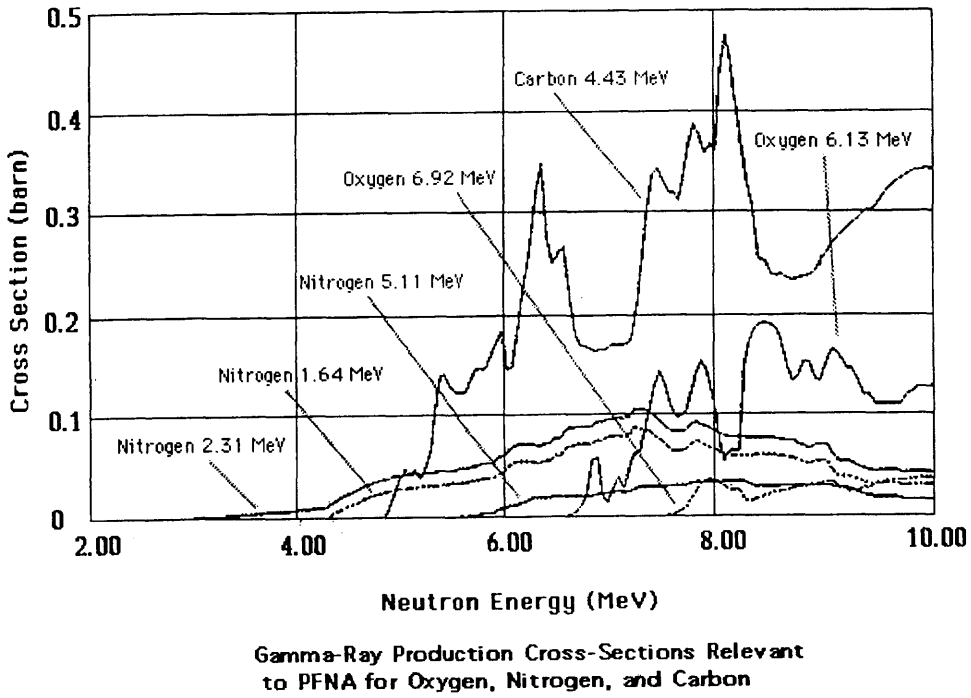

Figure 2.3 Fast Neutron Cross Sections

The cross section represents the probability of incident neutron interacting with matter. It is strongly energy dependent. Roughly speaking, the neutron interaction rate and the prompt gamma ray production rate are proportional to the neutron flux, cross section, and elemental density.

When mono-energetic neutrons interact with matter, a continuous spectrum is quickly formed (because of elastic scattering). That is, neutrons of different energy are always the situation that the target nuclei experience. The complexity of energy dependence of cross section leads to difficulty in calculating gamma ray output and therefore simulation methods are usually used. Later we will give the Monte Carlo simulation results.

2.2.2 Neutron Source

Inelastic scattering and most fast neutron reactions have negative Q-value. That is, they absorb the kinetic energy of incident neutrons. The source neutron must have energy higher than the corresponding threshold energy. That is about 3Mev for Nitrogen and 5-7Mev for Carbon and Oxygen. Isotope neutron sources are not suitable for our use.

The requirements for the neutron source are:

- (a) Maximum neutron energy is above Oxygen threshold;
- (b) There is no neutron of energy below Nitrogen threshold;
- (c) Intensity is high. 10^8-10^9 neutrons per second are necessary.
- (d) The source operates in pulsed mode. It's important to separate fast neutron induced gamma rays and thermal neutron induced gamma rays.
- (e) Cost is relatively low.

A good choice is the compact D-T neutron source, based on the nuclear reaction

$$^2H + ^3H - n + ^4He + 17.59Mev.$$

The reaction has a positive Q-value. The deuteron ions are usually accelerated to 100kev-400kev energy for higher reaction cross section (up to 5 barns) and adequate penetration into tritium target, and for higher neutron yield.

For bombarding energies below 400kev the angular distribution of the emitted neutrons is nearly isotropic in the center of mass system. In the laboratory coordinates, differential cross-sections in the forward direction are about 25% higher than in the backward direction at deuteron energy of 400kev. So it is always advantageous to use neutrons in the forward direction [7]. The energy of neutron in the laboratory system is 14.8Mev in the forward direction. Figure 2.4 shows such a neutron source.

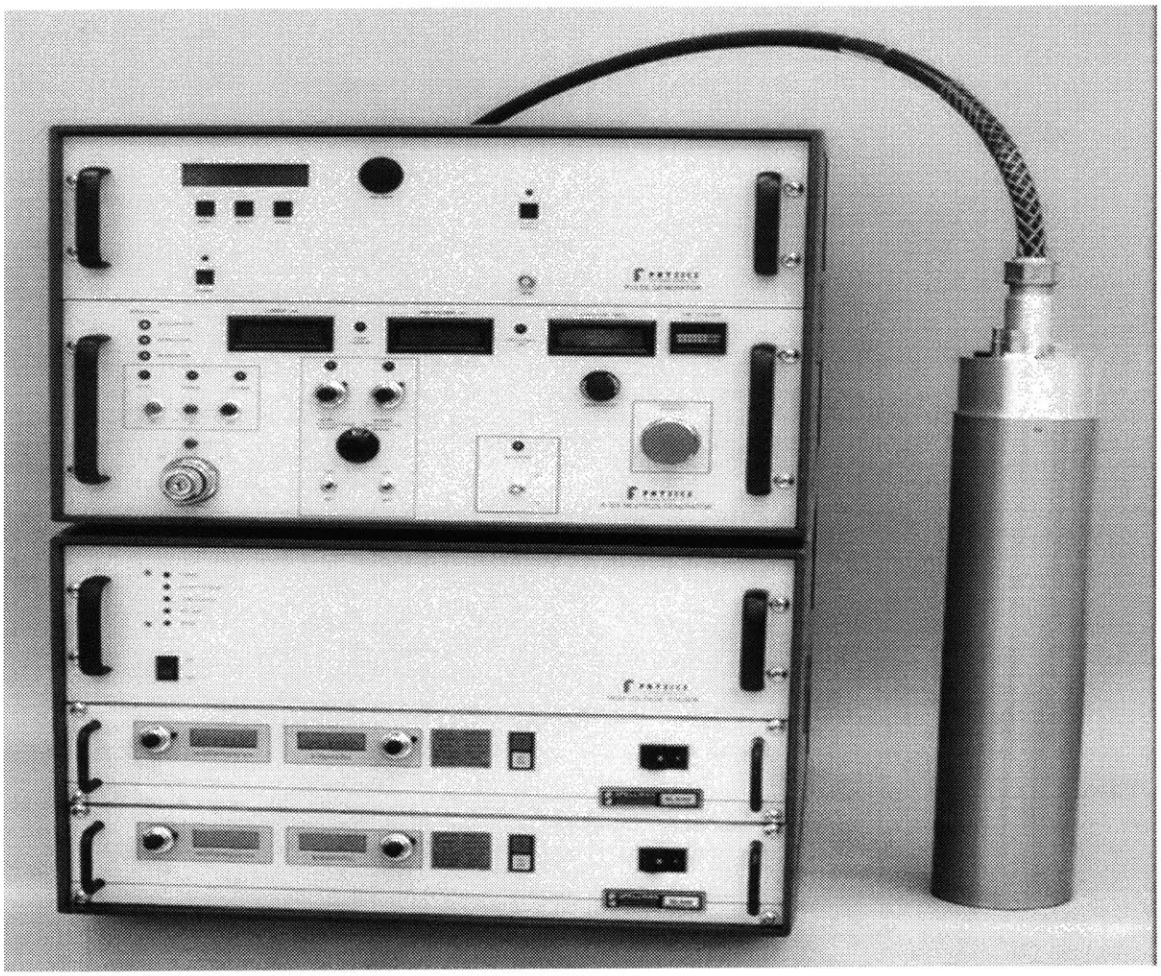

Figure 2.4 A compact D-T neutron Source

2.2.3 Neutron Penetration

It is desirable to have a neutron field of nearly uniform flux. In such a situation, intensity of prompt gamma rays of certain energy is proportional to the density of corresponding element over the field of view. If the non-uniformity is large, compensation methods may not work very well, if at all.

We studied with MCNP-4A code the penetration of source neutron into a large suitcase (See Figure 2.2), and the result is given in Table 2.2.

Table 2.2 Neutron Fluence of Different Energy Group (#/cm^2)

Energy range	Fluence	Percent
2.3Mev-4.4Mev	7.33×10^{-7}	7%
4.4Mev-13.9Mev	3.45×10^{-6}	32%
13.9Mev-14.1Mev	6.50×10^{-6}	61%
Total	1.07×10^{-5}	100%
Flux at 80cm without any material	1.24×10^{-5}	--

A 30cmX60cmX80cm suitcase full of wool (density: 0.18g/cm^3) except in the center there is a TNT sphere with a radius 3cm. The point neutron source sits 50cm away from the 30cmX80cm surface (and therefore 80cm away from the center of suitcase). The neutron fluence inside the TNT sphere is tallied for different neutron energies, as given in table 2.2. The tally is normalized to per source neutron. Neutrons in the 13.9Mev-14.1Mev group are those unscattered, or arriving directly from the source.

Of the total fast neutron fluence, more than 60 percent is from unscattered neutrons. And the total fast neutron fluence (1.07×10^{-5}) is close to that without any material (1.24×10^{-5}). Because the suitcase is the typical size and weight, we may conclude that fast neutrons have adequate penetrating power for large passenger suitcases and that the non-uniformity in fast neutron fluence is only

(1.24-1.07)/1.24 = 14%.

In addition, after penetrating inside, the neutrons have lower average energy and thus higher gamma ray production cross section. This effect compensates the non-uniformity and we can expect a gamma ray source distribution nearly proportional to elemental distribution.

2.2.4 Induced Gamma Ray Spectra

(a) Fast Neutron Induced Gamma-Ray

Fast neutrons induce prompt gamma ray by inelastic scattering or reaction [4][5][6]. Table 2.3 gives the major lines of fast neutron induced gamma rays. Gamma rays may be scattered inside the object itself, and therefore the output spectra are continuous between the major lines.

Table 2.3 Fast Neutron Induced Gamma Rays

Energy (Mev)	Element	Origin
0.51	O	$^{16}O^*$: 6.03Mev--0 via pair
0.72	N	$^{14}N^*$: 5.83Mev--5.11Mev
1.63	N	$^{14}N^*$: 3.95Mev--2.31Mev
2.12	N	$^{14}N(n, \alpha)^{11}B^*$: 2.14Mev--0
2.20	H	$^{2}H^*$: 2.2Mev--0
2.31 ***	N	$^{14}N^*$: 2.31Mev --0
2.74	O	$^{16}O(n, \alpha)^{13}C^*$
2.79	N	$^{14}N^*$: 5.10--2.31Mev, $^{11}B^*$:5.03--2.41Mev
3.08	O	^{16}O (n, α)$^{13}C^*$
3.38	N	$^{14}N^*$: 5.68Mev--2.31Mev
3.68	O	$^{16}O(n, \alpha)^{13}C^*$

3.85	O	^{16}O (n, α)^{13}C*
4.43 ***	C	^{12}C*: 4.43Mev--0
4.91	N	^{14}N*: 4.91Mev--0
5.01	N	^{14}N (n, α)^{11}B*: 5.03Mev--0
5.10 ***	N	^{14}N*: 5.10Mev--0
5.69	N	^{14}N*: 5.69Mev--0
5.83	N	^{14}N*: 5.83Mev--0
6.09	N	N14(n, p)C14*: 6.09Mev-0
6.13 ***	O	O16*: 6.13Mev-0
6.44	N	N14*: 6.44Mev-0

Figure 2.5 gives the simulated gamma-ray spectrum from a 40cmx50cm surface of the suitcase, which is 25cmX40cmX50cm in size. A TNT sphere of radius 5cm sits at the center, surrounded by 3cm thick Nylon. Other space inside the suitcase in filled with wool (0.18g/cm^3). The 14Mev Neutron source is 30cm away from the 25cmX50cm surface, and gamma rays tallied are from the 40cmx50cm surface. The effect of gamma ray scattering inside the object is taken into account, so the spectrum is continuous rather than separate lines. Table 2.4 gives the yield of major gamma rays, in units of gamma rays per source neutron.

Table 2.4 Fast Neutron Induced Gamma-Ray Yield

Energy	C 4.43Mev	N 2.31Mev	N 5.10Mev	O 6.13Mev	Total
TNT	2.5×10^{-7}	4.9×10^{-8}	3.2×10^{-8}	1.1×10^{-7}	3.8×10^{-7}
TNT + Nylon	2.5×10^{-7}	4.7×10^{-8}	3.1×10^{-8}	1.0×10^{-7}	3.4×10^{-7}
TNT +Nylon +Wool	2.9×10^{-7}	5.9×10^{-8}	3.6×10^{-8}	1.3×10^{-7}	3.8×10^{-7}

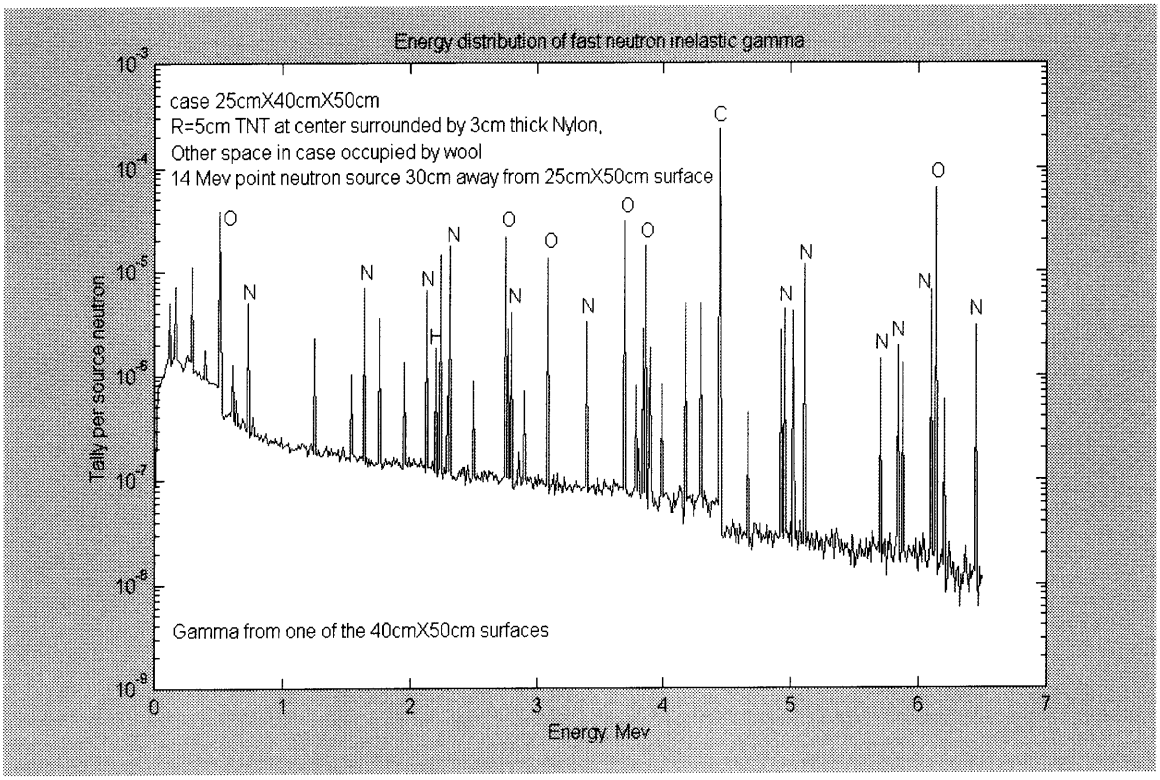

Figure 2.5 Fast Neutron Induced Gamma Ray Spectrum (TNT)

(b) Thermal Neutron Induced Gamma-Ray

Some of the incident neutrons get thermalized in the inspected object and induce prompt gamma ray by capture. Hydrogen and Chlorine have large capture cross-sections. The simulated gamma-ray spectra of Cocaine Hydrochloride are given in figure 2.6. Both fast neutron induced and thermal neutron induced gamma rays are considered.

Again the spectra are those with gamma ray scattering taken into account (Otherwise, they would not be continuous.). Gamma rays form one 200cmx154cm surface are tallied, in the unit of gamma rays per source neutron.

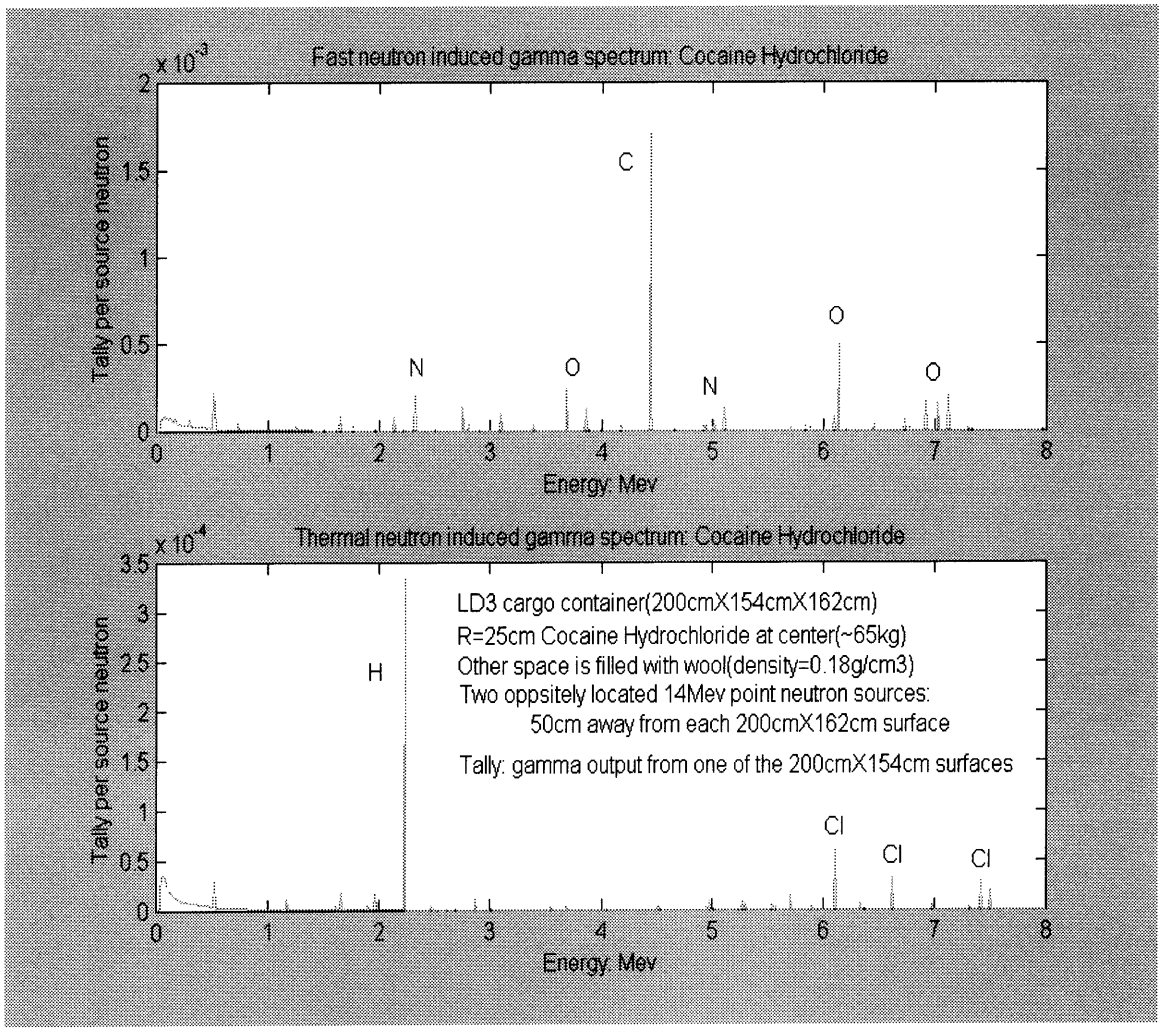

Figure 2.6 Neutron induced gamma rays for cocaine hydrochloride.

(c) Angular Distribution

Generally, the angular distribution of single emitted gamma rays is not isotropic. In our arrangement, the incident neutron has 14.8Mev energy, well above the threshold of gamma ray emitting processes. Neutrons may have been elastically scattered once or more before inducing a gamma ray. This randomization results in a nearly isotropic distribution of gamma ray. We may put our detector away from in neutron incident direction, as shown in figure 2.2

2.2.5 Summary

Explosives and drugs have distinctive elemental content. Prompt gamma rays are induced by neutron interactions with different elements. By imaging the out-coming gamma rays, we get a mapping of elemental distribution.

Fast neutron induced prompt gamma rays provide us the means of locating Carbon, Nitrogen and Oxygen. In addition, thermal neutron Induced prompt gamma rays enable us to locate Hydrogen and Chlorine.

The neutron source is to operate in pulsed mode. The beams-on time is several microseconds, and during this period, the fast neutron induced gamma rays are imaged. During the interval, thermal neutron induced prompt gamma rays are imaged.

Chapter 3 Coded Aperture Imaging

An imaging method is needed to obtain the spatial distribution of gamma-ray sources, and therefore of different elements. In this chapter we briefly introduce Coded Aperture Imaging method.

3.1 Basic Concept

Coded Aperture Imaging method was first proposed by Mertz and Young [9], and significantly improved by Barrett [8], who used an Uniformly Redundant Array coding mask. The basic idea is illustrated in figure 3.1.

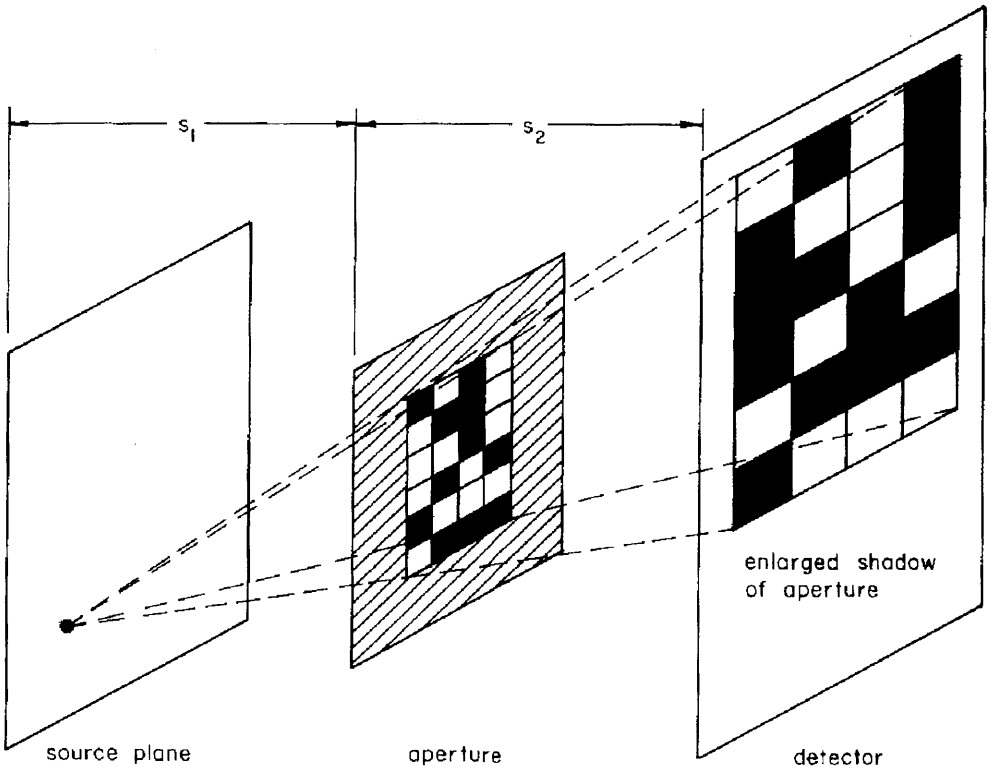

Figure 3.1 Coded Aperture system for photon imaging

The coding mask (aperture) is made in gamma-ray attenuating material with a carefully selected pattern. For our purpose, the material is lead, which covers the black regions on the mask (aperture). The white region on the mask (aperture) has no lead and is therefore transparent to gamma rays.

As shown in figure 3.1, a point source casts a magnified shadow of the mask onto the detector, which is location-sensitive. In principal, the shadow contains the following information:

- (a) The size of the shadow can be used to determine the longitudinal coordinate (z or s1) of the source.
- (b) The lateral coordinates of the center of the shadow on the detector, with the help of longitudinal coordinate, give the lateral coordinates of the source (x and y).
- (c) The total number of detected gamma rays is proportional to the source intensity.

Coded Aperture Imaging is a two step process. The first step, encoding, is just geometrical shadow casting. The second step (decoding) is carried out by a computer, which extracts source distribution from the information recorded on the detector.

The coding mask can be either 1-D or 2-D. (The detector is correspondingly 1-D or 2-D.) 2-D mask and detector enable us to locate a 3-D source distribution, as shown in figure 3.1. 1-D mask and detector, which is in the plane of paper as in figure 3.1, lead to the reconstructed 2-D source distribution in the plane of paper.

3.2 Decoding and Uniformly Redundant Arrays

The reconstructed imaging may be denoted as:

$$r(x, y, z) = s(x, y, z) \otimes h(x, y, z)$$

That is, the reconstructed image r(x, y, z) is the convolution of the source distribution s(x, y, z) and the system response h(x, y, z), which is also called Point Spread Function (PSF). The PSF h(x, y, z) is the auto-correlation function of the mask pattern.

When a 2-D mask and detector is used, the following procedure leads to the reconstructed 3-D imaging:

- (a) Record the shadow on the detector.
- (b) Reconstruct a slice of the object with a fixed z value.
- (c) Repeat (b) with other z values.
- (d) Combine all slices to obtain the 3-D image.

When a 1-D mask and detector are used, everything is done in the plane of paper, or y-z plate. There is no x coordinate, which points inside the paper in figure 3.1.

An URA coding mask is composed of several mosaics of a basic pattern, which is pseudo-random. The repetition number n of the basic pattern in each dimension (x or y) is usually required to be at least 2. If n is bigger, the field of view is bigger. Whatever n is, the detector must hold the shadow of one basic pattern.

For near field source, which is our case, an Uniformly Redundant Array mask is optimal in term of Point Spread Function [][][]. Its auto-correlation function has a sharp main lobe and the side-lobes are spatially uniform. A 1-D example is given in figure 3.2.

An important property of uniformly redundant codes is that their auto-correlation functions have a sharp central peak surrounded by side-lobes of uniform height over a substantial region. If the object is not too large, the effect of the side-lobes is to produce a uniform background level that can be remove by subtracting a constant bias level from the imaging.

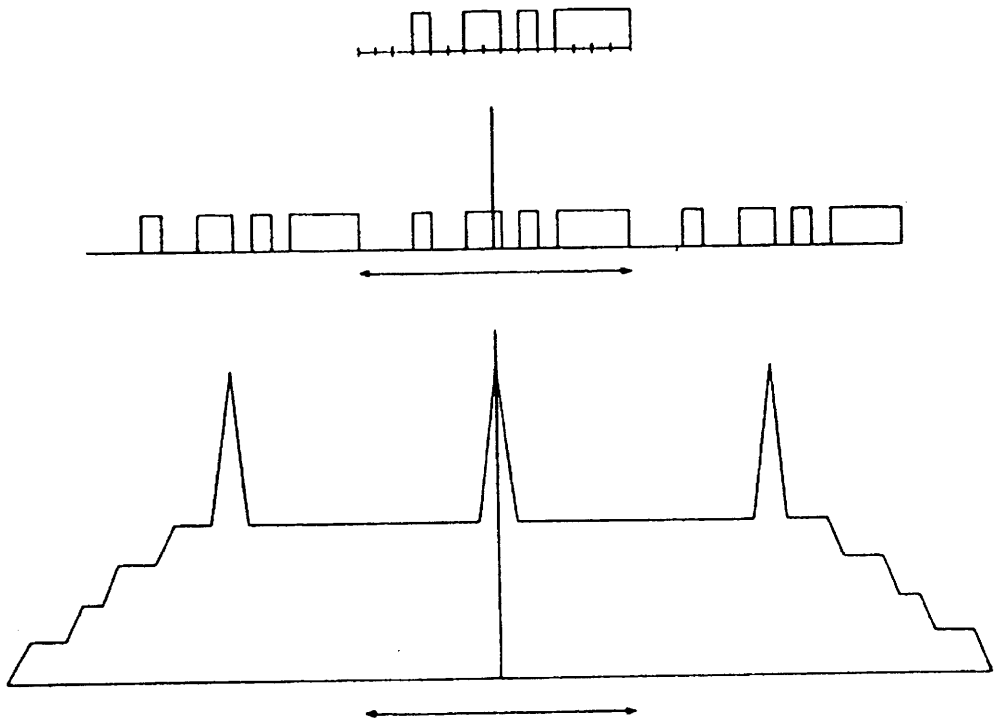

Figure 3.2 1-D URA mask and its decoded PSF

Top: The mask pattern. Center: Cyclically repeated version of basic pattern.

Bottom: PSF, which is the convolution of the top and the center.

3.3 Laminography

Multi-plane sections can be obtained from a single view (data collection) with a single coding mask. This is also called Laminography [11].

Coded Aperture Laminography is a focusing technique to imaging different layers of an object (gamma-ray source in our application). While all parts of the object contribute to the collected data, as mentioned in the description of reconstruction algebra, only one slice of object is reconstructed with a fixed z value—other slices are all blurred out.

By reconstructing different slices using different z values, we obtain the 3-D imaging from a single view.

A corresponding disadvantage is that the out-of-focus planes do not necessarily blur smoothly and continuously, but may exhibit sharp structure and even negative values. These tomographic artifacts are to be studied carefully in our future work.

Much of the early impetus for research into coded aperture imaging arose from the large increase in geometrical collection efficiency that they afford. A pinhole collimator has an efficiency as low as 10^{-4}. A typical URA mask has half of its area transparent and has a geometrical efficiency of 100 times larger. For a point gamma-ray source, this means that the data acquisition time can be reduced by the same factor without losing signal-to-noise ratio (SNR). The SNR situation becomes less favorable for an extended object. As more source points are added to the object scene, each detected photon conveys less information because of the overlapping aperture shadows it is associated. Generally speaking, coded apertures collect more photons than conventional apertures, but also require more for the same SNR. This factor is under careful study in our group.

Chapter 4 General Requirement of Detectors

So far we have introduced Fast Neutron Analysis and Coded Aperture Imaging. A key issue is the designing of a high-energy gamma ray imaging detector.

4.1 Gamma Ray Detectors

4.1.1 Gamma-Ray Interactions

Gamma ray must interact with detector material in order to be recorded. There are three major types of interactions: Photoelectric absorption, Compton scattering, and Pair production. The cross-section of gamma-ray interactions with sodium iodide is given in figure 4.1 [12].

(a) Photoelectric Absorption

In the photoelectric absorption process, a photon (gamma ray) undergoes an interaction with an absorber atom in which the photon completely disappears. In its place, the atom ejects an energetic photoelectron from one of its bound shells. The photoelectron then loses its kinetic energy in the detector, causing measurable effect.

Photoelectric absorption leads to a full energy peak in the recorded pulse height spectrum. In the gamma-ray energy of above 2Mev, which is our case, the contribution of direct photoelectric absorption is negligible.

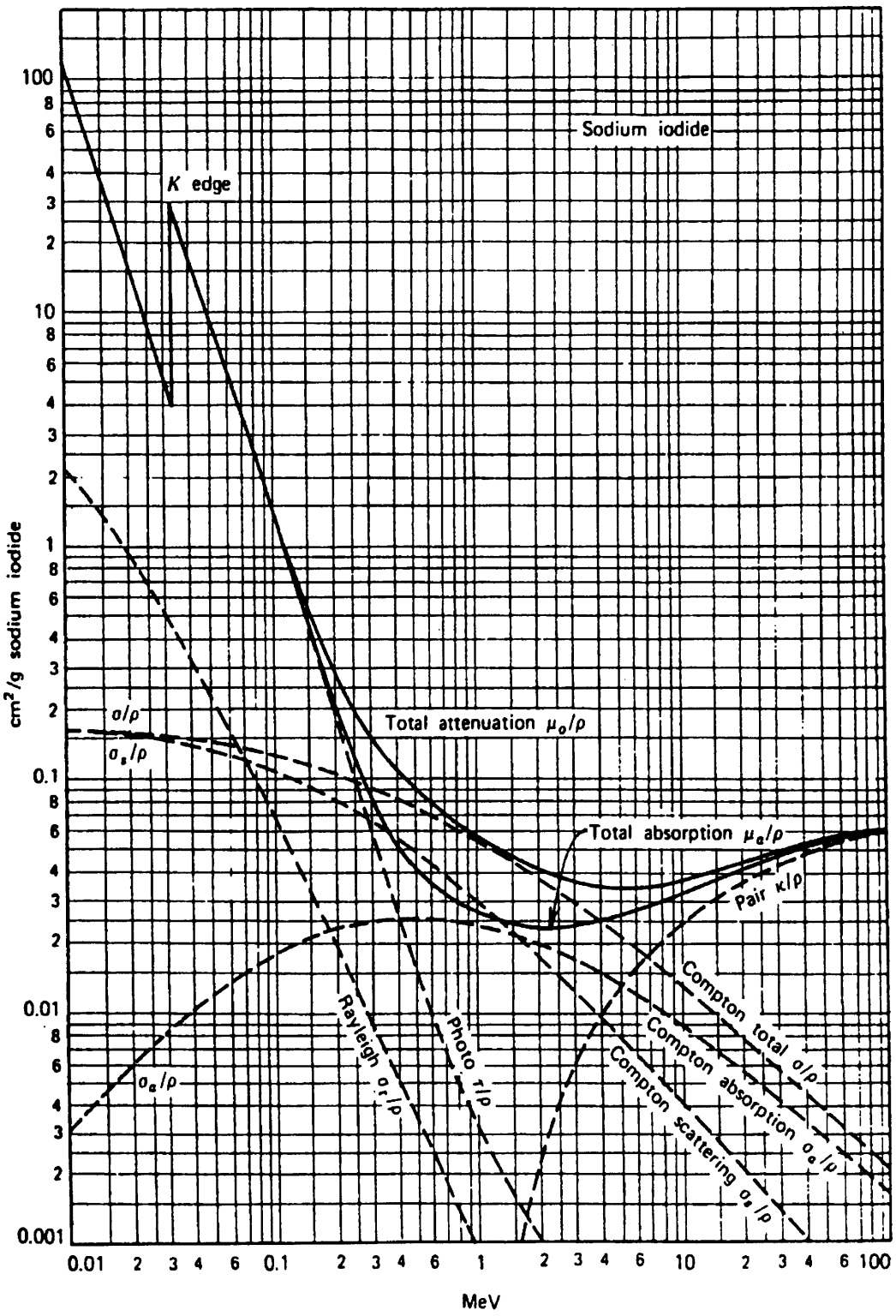

Figure 4.1 Gamma-ray cross-section in NaI

(b) Compton Scattering

The interaction process of Compton scattering takes place between the incident gamma-ray photon and an electron in the absorbing material. It is the predominant interaction mechanism for medium energies. In Compton scattering, the incoming photon is deflected through an angle with respect to its original direction. The photon transfers a portion of its energy to the electron, which is known as a recoil electron. Because all angles of scattering are possible, the energy transferred to the electron can vary from zero to a large fraction of the gamma-ray energy. As in the photoelectric absorption, the secondary fast electron then deposits its kinetic energy in the detector material and causes measurable effect. The scattered photon also has a possibility to interact with the detector material before escaping.

Compton scattering makes the recorded pulse height spectrum continuous and therefore complicated. It is therefore less desirable in imaging.

(c) Pair Production

If the gamma-ray energy exceeds twice the rest-mass energy of an electron (1.02Mev), the process of pair production is energetically possible. Pair production is important when the incident gamma-ray energy is above 4-5Mev for most detector material. In the interaction, which takes place in the coulomb field of a nucleus, the photon disappears and is replaced by an electron-positron pair. The energy of incident photon is partly (1.02Mev) transferred to rest-mass energy of the electron-positron pair. Other energy is shared by the pair as kinetic energy. The kinetic energy carried by the electron-positron pair causes measurable effect. The positron will subsequently annihilate after slowing down in the absorption medium, giving two annihilation photons, both of energy 0.511Mev. Either of the two photons may or may not interact further with the detector material.

Pair production leads to three peaks in the measured spectrum: full energy peak, single escape peak, and double escape peak. Detector material with higher atomic number (Z) has larger pair production cross-section.

4.1.2 Measurable Effects

The gamma ray itself causes no direct effect that leads to the recording of the event. The secondary fast electrons, which are produced in one of the three interactions described above, must cause some measurable effects in the detector in order to be recorded. There are two types of effects: Ionization and Scintillation. (Cherenkov Radiation is not discussed here.)

(a) Ionization

When a charged particle travels in an absorbing medium, it interacts simultaneously with many atomic electrons. In any one such encounter, the electron feels an impulse from the Coulomb force as the incident particle (secondary fast electron if gamma ray is the incident radiation) passes its vicinity. Depending on the proximity of the encounter, this impulse may be sufficient either to raise the electron to a higher-lying shell within the absorber atom (excitation) or to remove completely the electron from the atom (ionization). The energy that is transferred to the electron must come at the expense of the incident charged particle, and its speed is reduced as the result of encounter. The primary particle must lose its energy in many such interactions during its passage in the absorber. At any given time, the particle is interacting with many electrons, so the net effect is to decrease its speed continuously until the particle is stopped.

The products of these encounters in the absorber are either excited atoms or ion pairs. Each ion pair is made up of a free electron and the positive ion of an absorber atom from which an electron has been totally removed. The average energy needed to produce an ion pair is about 3ev in semiconductor detectors and about 30ev in gas detectors. The detector then collects these ion pairs (In some detectors, they are even multiplied.), giving an electric signal.

(b) Scintillation

As in the Ionization process, The energetic charged particle deposits its kinetic energy in the medium and causes excitation (and maybe ionization). In organic material, the molecules are excited, and in inorganic material the lattice is excited.

In scintillation material, the excitation leads to the emission of visible light. This light is then collected and amplified by a Photo Multiplying Tube (PMT) to give an electric signal.

4.1.3 Operation Modes

Detectors work in three general modes: pulse mode, current mode, and mean square voltage mode.

Pulse mode is the basic mode of operation. Each individual incident particle causes ionization or scintillation, which in turn leads to an electric pulse. The electric pulse lasts for a period of less than $1\mu s$ for some scintillators and up to $100\mu s$ for gas detectors.

If the multiplication of ionization by gas or scintillation by PMT does not go to saturation, the amplitude of resulting electric pulse is proportional to the energy deposited by the incident particle. So in pulse mode, the energy and timing information of individual events are preserved.

In current mode, the detector collects the total ionization caused by all individual events. The time constant is on the order of seconds. The output thus corresponds to the total energy deposited by all incident particles. Information about any single event is lost. Current mode works for high event rates.

Mean square voltage mode (also known as Campbell mode) is an extension of current mode. By high-pass filtering the current, The signal (mean square signal) is directly proportional to the event rate and the square of the charge produced in each event. This mode is useful in mixed radiation environments—it is mostly used in reactor instrumentation.

4.2 Requirements

The detector we need must have adequate spatial resolution to image the gamma rays, and adequate energy resolution to tell gamma rays of different energy (therefore from different elements). High detection efficiency is also expected.

These requirements basically rule out gas detectors and semiconductor detectors. Inorganic scintillators are the practical choices. Later on we will mostly discuss NaI(Tl) and BGO scintillators. Table 4.1 gives basic properties of NaI(Tl) and BGO scintillators [12][19].

Table 4.1 Properties of Scintillators

Material	NaI(Tl)	BGO
Density (g/cm^3)	3.67	7.13
Emission Maximum λ_m (nm)	415	505
Refraction Index at λ_m	1.85	2.15
Principal Decay Constant (μs)	0.23	0.30
Total light yield (photon/Mev)	38000	8200
Relative γ ray pulse height	1.00	0.23

4.2.1 Range, Spatial Resolution and Size

Spatial resolution can be reached in two ways: (a) Use an array of small detectors, each working independently. The size of small detector defines the spatial resolution. (b) Use a large area detector and let the ionization or scintillation distribute itself to several collecting terminals (electrodes or PMTs). The location of event may be calculated with these outputs.

In our application, the spatial resolution of detector is desired to be about 1 or 2 centimeters. Let is study the edge effects of a 2.5cmx2.5cm by 10cm thick NaI(Tl) detector.

(a) Electron edge

The Compton electrons or pair production electrons (positrons) can have a kinetic energy of up to 5Mev for 6.13Mev gamma ray, the major line from Oxygen. They must deposit

all kinetic energy in the detector material to cause an effective counting. That is to say that they should not escape. Unfortunately, the range of these electrons is about 5mm in NaI. [12][19]

And as a result, only the inside 1.5cmx1.5cm part of the total 2.5cmx2.5cm area does not exhibit edge effect in terms of electron (positron) penetration. This not only largely reduces the counting efficiency, but also degrades the spatial uniformity.

(b) Gamma-ray edge

We would like that most recorded events fall into the full energy peak. That is, the incident gamma rays deposit all energy in the detector. This requires further interaction of Compton scattered photons or annihilation photons with the detector material.

Annihilation photons have energy of 0.511Mev and an attenuation of $0.09cm^2/g$ in NaI (figure 4.1). After travelling 2.5cm, 44 percent of these annihilation gamma rays remain non-interacted. The full energy efficiency can thus be expected very low for a detector as small as 2.5cmx2.5cm.

Figure 4.2 and 4.3 give the simulated response of detectors of different size and material. The gamma ray source is roughly the output of FNA gamma rays in figure 2.5.

An array of small detectors is not only costly, both in itself and the electronics, it simply does not work due to the edge effects.

As we encountered previously, the detector must be big enough to hold the shadow of at least one basic pattern of the coding mask. This generally requires a total size of 80cmx80cm or larger (2-D mask and detector).

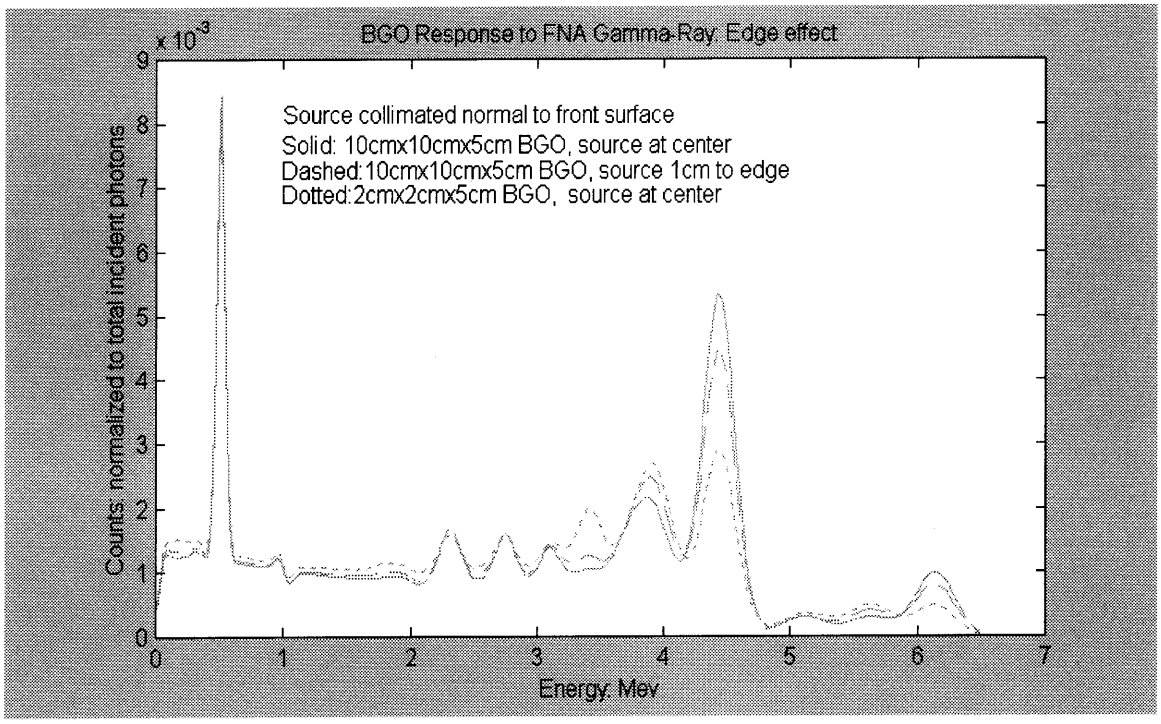

Figure 4.2 Detector Response (Different Sizes)

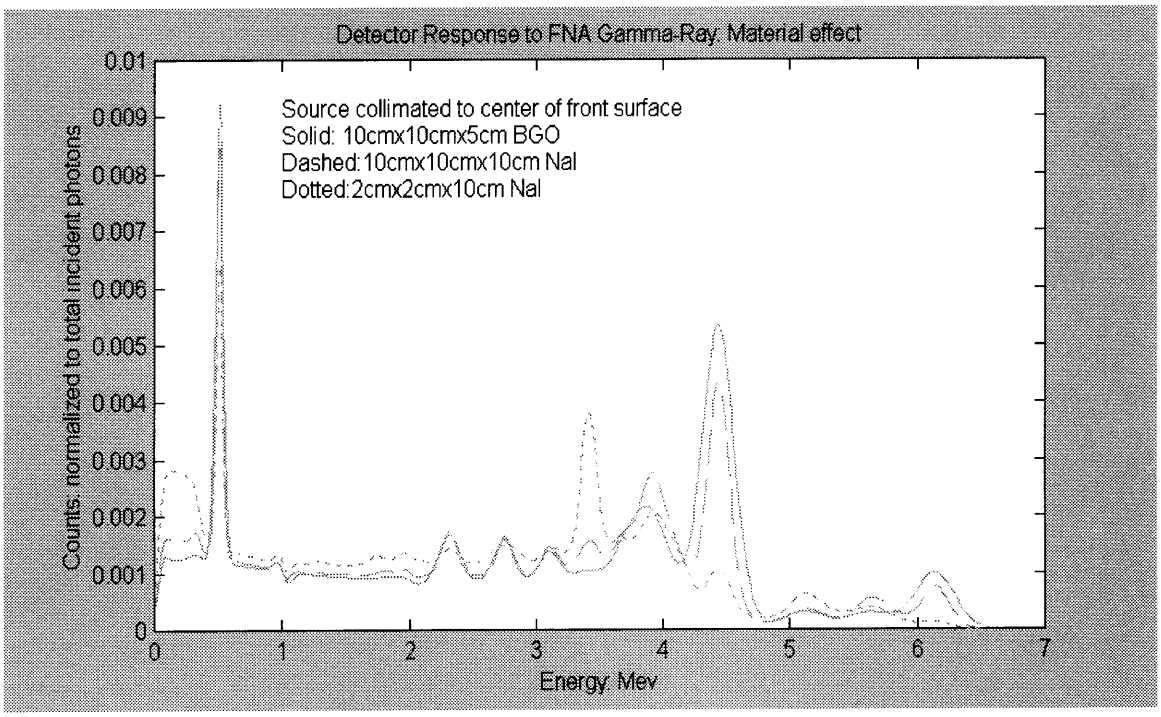

Figure 4.3 Detector Response (Different Materials)

4.2.2 Efficiency and Thickness

The total detection efficiency and peak efficiency depend on scintillator thickness because of the exponential absorption law. Thicker scintillator is better for efficiency, but worse for light sharing and thus spatial resolution, as we will discuss in the next two chapters. Figure 4.4 gives the thickness dependence of efficiency for BGO. Table 4.2 gives data for all detectors studied. In this study, gamma ray source with a spectrum of that in figure 2.5 is used. The beam is incidents normally onto the front surface center except in the case marked with edge, in which the incident point is 1cm from one side surface.

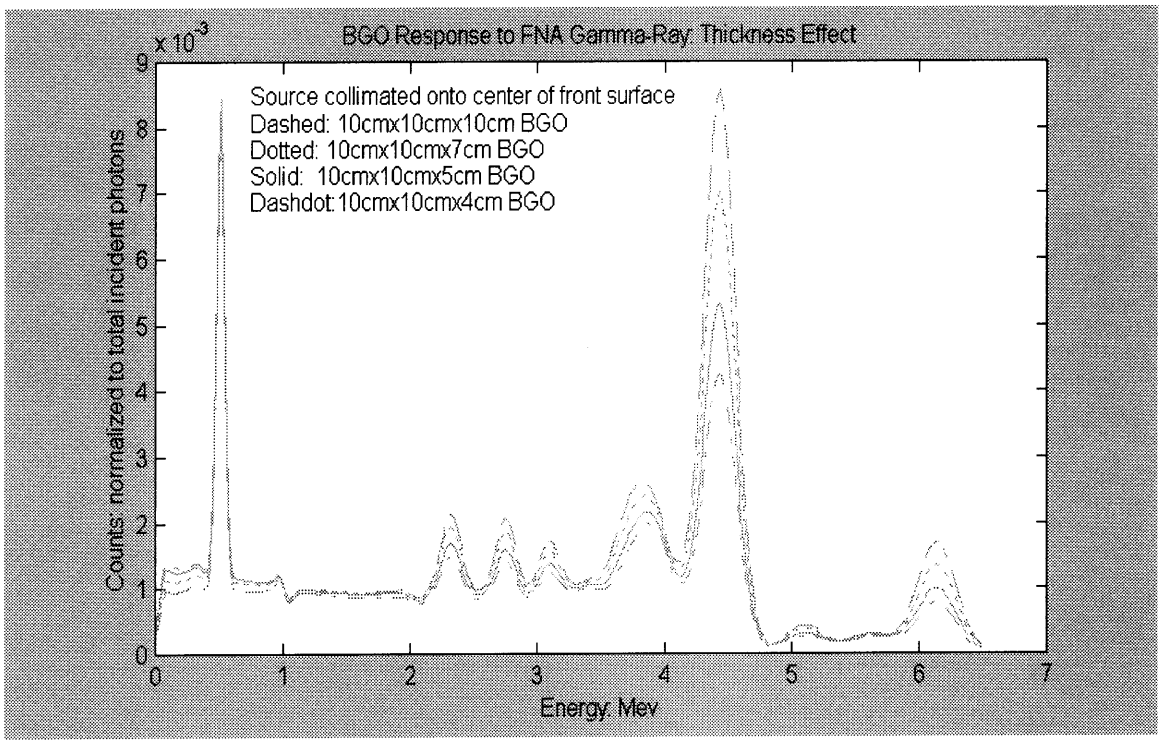

Figure 4.4 Thickness dependence of efficiency

Table 4.2 Peak Counts (Per Source Photon) for Several Detectors

	10^2x 10cm^3 BGO	10^2x 7cm^3 BGO	10^2x 5cm^3 BGO	10^2x 5cm^3 BGO, EGDE	2^2x 5cm^3 BGO	10^2x 4cm^3 BGO	10^2x 10cm^3 NaI	2^2x 10cm^3 NaI
Total Efficiency	0.95	0.88	0.79	0.79	0.79	0.72	0.76	0.76
4.43Mev SO	34%	34%	34%	34%	34%	34%	34%	34%
DP	-	-	-	0.002	0.010	-	0.003	0.030
SP	0.019	0.021	0.022	0.030	0.036	0.022	0.024	0.016
FP	0.250	0.203	0.153	0.126	0.079	0.121	0.089	0.019
5.10Mev SO	2%	2%	2%	2%	2%	2%	2%	2%
DP	-	-	-	-	0.001	-	-	0.002
SP	0.001	0.001	0.001	0.002	0.002	0.001	0.002	0.001
FP	0.015	0.012	0.009	0.007	0.005	0.007	0.006	0.002
6.13Mev SO	9%	9%	9%	9%	9%	9%	9%	9%
DP	-	-	-	-	-	-	-	-
SP	0.006	0.007	0.007	0.010	0.011	0.007	0.008	0.005
FP	0.063	0.051	0.037	0.030	0.018	0.029	0.020	0.003

SO: source fraction. Source of the whole spectrum is normalized to unity.

DP: double escape peak counts.

SP: single escape peak counts.

FP: full energy peak counts.

Edge means that gamma rays incident point is 1cm away from one side surface. (Still normal onto the front surface)

4.2.3 Energy Resolution

A fast electron gives on average 40 photons (visible light) per 1kev energy in NaI(Tl). In the gamma-ray energy range of 2-6Mev, the statistical fluctuation of collected photons contributes little to energy resolution. Actually, energy resolution in such situation is mainly decided by the spatial non-uniformity of photon collection. Given the complexity of FNA gamma-ray spectrum, an energy resolution of ~8% is necessary for 2-6Mev. This is one of the major concerns in detector design.

4.3 Neutron Irradiation

The detector is at a finite distance from the neutron source, and therefore may be irradiated by fast neutrons. Both Iodine in NaI(Tl) and Germanium in BGO have a considerable activation cross-section [7], and Oxygen (Which exists in BGO) is the element of interest in the object, which might cause a problem.

In figure 2.2, the detector is off the original neutron beam by 90 degree. Such an arrangement reduces the neutron flux at detector, and also neutrons scattered to the detector have much lower energy, unlikely to excite 6.13Mev gamma ray from oxygen [3][4][5][6].

Chapter 5 NaI(Tl) Detector Design

As we mentioned in last chapter, one important concern in organizing the imaging system described in chapters 2&3 is the detector design. Gamma rays of 4-6Mev energy interact with matter via Compton scattering or pair production, so after the original interaction, the detector must record the kinetic energy carried by Compton electron or electron/positron pair, and also caught the scattered photon or the two photons from positron annihilation. Small size single detector has very low peak efficiency compared with others, simply because it is too small to absorb all electron energy (The range of fast electron is 5 millimeters, thus sever edge effect exists), let alone to hold any second events. If we are to put a lot of single detectors together, we must choose small detectors for good spatial resolution while large detectors for high efficiency. That is the basic trade off. An array of single detectors does not work. In addition, its cost is prohibitive.

In this Chapter, we propose a NaI(Tl) detector assembly that uses the light-sharing technique, suitable for the imaging process described in previous chapters.

5.1 Possible Installations

In Anger Camera [10], a large NaI(Tl) crystal is used. Scintillation light is distributed to several Photo-Multiplier-Tubes(PMTs) and the location of scintillation is calculated with the PMT outputs. Because the gamma energy is only 140kev, the crystal is relatively thin. In PET, 2.5cm-3cm thick BGO is used, and the crystal is usually cut into pieces with light reflector between them. Scintillation light is first collimated in the crystal pieces and then distributed in the light guide. The spatial resolution is the size of BGO pieces. Casey gave a theoretical analysis of this arrangement [15], while Derenzo gave simulation study for NaI(Tl) system used in SPECT [16].

We are to detect 2 to 6Mev energy gamma rays, thus a crystal thickness of about 10cm is needed for reasonable detection efficiency. At this crystal thickness, collimation as well as distribution of scintillation light is necessary, as in the block arrangement of PET

detectors. For this method, we cut the crystal into small pieces. An additional concern is that we need good energy resolution, since we are dealing with multi-energy gamma ray source.

Large phototubes usually have a non-uniform photo cathode response. We choose photo tubes of 7.6cm(3") in diameter, and light guide of 1cm thick or more is to be used between crystal and PMTs to further reduce the effect of photo cathode non-uniformity [12][14][18].

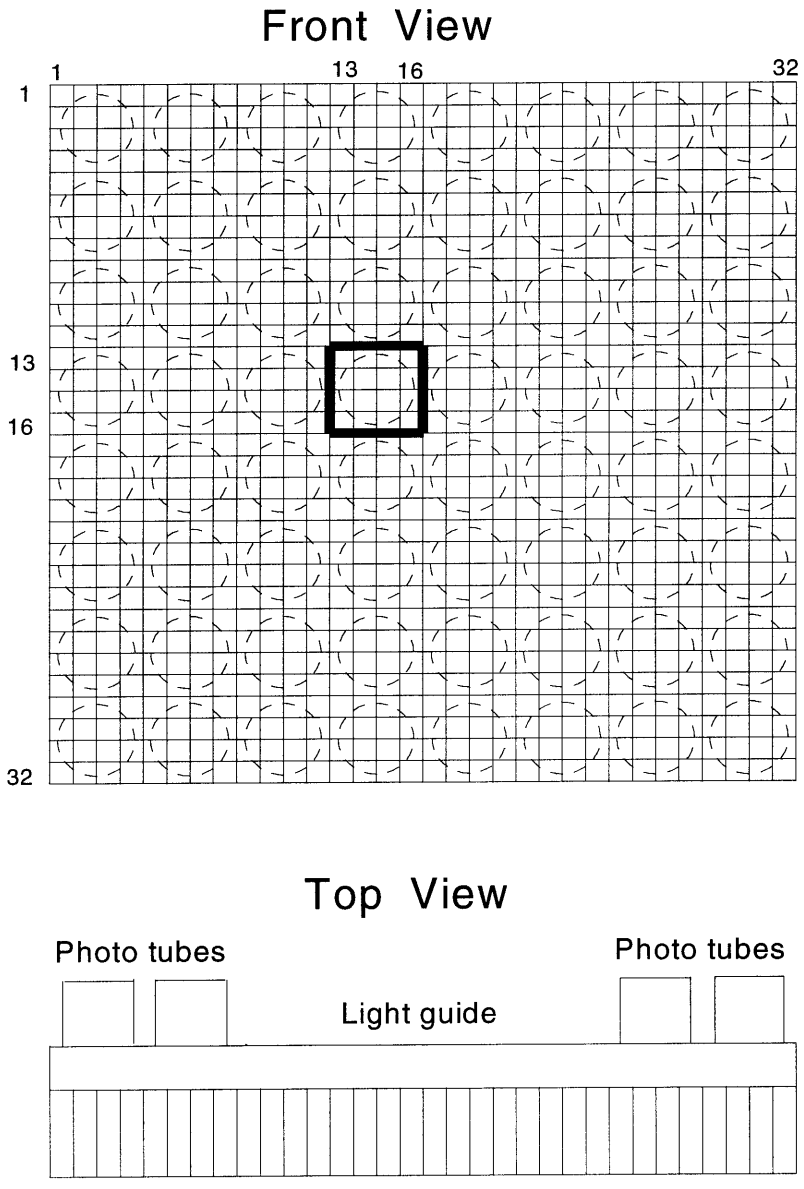

Figure 5.1: Sketch of NaI(Tl) Detector assembly

The detector assembly design is given in figure 5.1. The crystal is 80cm high, 80cm wide and 10cm thick, and it is cut into 2.5cmx2.5cmx10cm (10cm thickness) pieces forming a 32x32 matrix. The PMTs form an 8x8 matrix. By properly arranging the interfaces and boundary surfaces, we are to control the propagation of scintillation light so that:

- (a) With the PMT outputs, we can assign a count to the crystal piece where the scintillation event occurs, thus obtain a spatial resolution (cell width) of 2.5cm;
- (b) With the summation of all PMT outputs, we can determine the energy of incident gamma ray and assign a count to a specific element. An energy resolution of about 7% at 6.13Mev is needed.

We may follow the design of Anger Camera—do not cut the crystal at all, and come to the *single* crystal installation—the spatial resolution can be expected to be very poor. Or we may follow the design of PET detector, cut the crystal into pieces and apply powder reflector between pieces collimating scintillation light, then use a light guide to distribute the light. This is called *reflective* interface installation and its energy resolution can be expected to be very poor because of the depth dependence of total light output.

A novel idea is to distribute and collimate the scintillation light simultaneously—simply by making the interfaces partly transparent.

Diffuse interface installation is to make the crystal interfaces diffusive by sanding, without coating with anything, or an air gap. When light comes to the diffusive surface, it is re-directed isotropic, with no absorption.

Air-gap installation is to polish the surfaces, and leave an air gap (0.1mm thickness) between crystal pieces. Because the refractive index is unmatched, this sandwich structure is partly transparent. This design is not quite practical.

The out surface of crystal array is polished and coated with white reflector. The interface between crystal pieces and light guide is polished. The interface between light guide and phototube windows is also polished and the light guide surface uncovered by the phototube is coated with white reflector.

5.2 Modeling

We use Monte Carlo method to simulate the propagation of scintillation light for various installations. The meanings of several terms are given bellow:

- PIECE: the 2.5cmx2.5cmx10cm crystal elements
- INTERFACE: surfaces between *pieces*
- SOURCE: scintillation light source
- LOCATION: digitized X&Y coordinates of *piece*, ranging from 1 to 32
- DEPTH: Z coordinate of *source*, ranging from 0 to 10cm, a *depth* of 10cm is closest to light guide.
- PMT#: photo tube ID number (X: 1-8, Y: 1-8); when concerning 1-D distribution, PMT# refers to the column number (1-8) and output refers to sum of outputs in that column
- SINGLE: single large crystal installation as described above
- REFLECTIVE: reflective interface installation as described above
- DIFFUSE: diffusive interface installation as described above
- AIRGAP: *air-gap* sandwiched interface installation as described above

In the propagation of light, the following facts are assumed:

- Each scintillation event is represented by a point light source, located on the central line of a crystal piece. If no source depth is specified, the source is at the center of that crystal piece. This is not quite accurate because fast electrons/positrons may travel several millimeters in NaI(Tl).
- 100,000 photons are computed for each scintillation event. Typically a 2.5Mev gamma ray gives that amount of light [12[13]. These photons spread out isotropically.
- NaI crystal does not absorb the scintillation light.
- All photons are assigned a wavelength of 415nm, the emission maximum.

- The refractive indexes are taken as: NAI:1.85; Pyrex (light guide):1.5; Glass (PMT Window):1.5
- The average reflectivity of white reflector is taken as 90%. This is practical with titanium dioxide or magnesium oxide reflective powder, for the emission spectrum of thallium activated sodium iodide or NaI(Tl) [12][13].
- At polished surfaces, light undergoes either internal reflection or Fresnel reflection/refraction. Polarization is NOT considered.
- At diffuse surfaces, photons are scattered isotropically. At Reflective surfaces, which are coated with powder reflector, photons are either absorbed (with a probability of 10%) or scattered back isotropically.

5.3 Air-Gap Installation

We first give in detail the simulation results for air-gap Installation, and then as comparison the major results of other installations.

5.3.1 Distribution Pattern

Light spreads independently in X and Y directions. The propagation of light can therefore be described by two 1-D distributions. Figure 5.2 gives the 1-D distributions of light outputs. Light Source is at the center of crystal piece (13,13), (14,14), (15,15) or (16,16). Light outputs from each column of PMTs (Column number is denoted as PMT# in the figure) are summed to give the 1-D distribution. From figure 1 we see that each photo tube covers a 10cm by 10cm area or 4 by 4 crystal pieces and that PMT (4,4) covers the above mentioned crystal pieces. Light guide thickness is selected to be 4cm. It can be seen that (Please also refer to figure 1):

The 1-D distributions are all peaked in the 4^{th} column of PMTs, as they should be because PMT (4,4) covers the related crystal pieces.

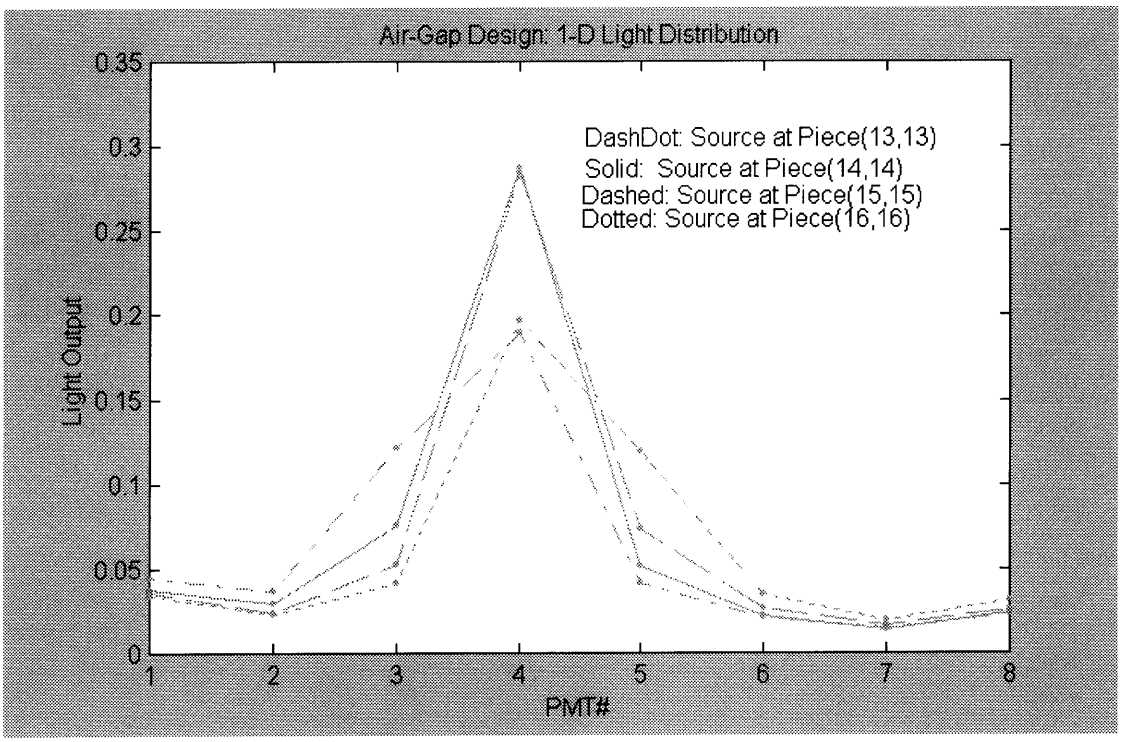

Figure 5.2: 1-D distribution of light output of selected pieces

The distributions for pieces (13,13) and (16,16) are wider than the other two because pieces (13,13) and (16,16) are only partially covered by the PMT while pieces (14,14) and (15,15) are completely covered by the PMT.

The distributions for pieces (13,13) and (16,16) are similar but flipped over, the same is true for pieces (14,14) and (15,15).

For pieces (13,13) and (14,14), outputs from 3rd column (left to peak) are larger than those from 5th column (right to peak) because the pieces are closer to column 3 PMTs than to column 5 PMTs. Similar results stand for pieces (14,14) and (15,15).

The 3rd column PMT output for piece (13,13) is larger than that for piece (14,14) while the 5th column PMT outputs for both pieces are about the same. This is because piece (13,13) is a direct neighbor of the column 3 PMTs while piece (14,14) is not. Similar result stands for pieces (15,15) and (16,16).

Outputs from column 1 and 8 are larger than we would expect. This is the edge effect. Our detector assembly is not (and need not to be) infinitely large.

The Peak/Total ratio (Ratio of output from peak column PMTs to total output), the Left/Total ratio (Ratio of the output from left-to-peak column PMTs to total output), and the Right/Total ratio (Ratio of output from the right-to-peak column of PMTs to total light output) are given in table 5.1.

Table 5.1 Peak Shape Ratios for Selected Pieces

	(13,13)	(14,14)	(15,15)	(16,16)
Left/Total	0.25	0.13	0.10	0.08
Peak/Total	0.38	0.53	0.53	0.39
Right/Total	0.09	0.09	0.14	0.24

We may process the data like this:

- From the total light output, determine the gamma ray energy.
- By locating the peak in the 1-D distribution, determine the PMT that covers the crystal piece of light source. In the above example, it's PMT (4,4).
- By calculating the peak/total ratio, decide whether the scintillation comes from one of the close-to-PMT-center pieces (in the above example, 14 or 15), or from one of the close-to-PMT-edge pieces (in the above example, 13 or 16).
- By calculating the left/total and right/total ratios, decide whether the source piece is to the left of the PMT center (in the above example, 13 or 14), or to the right (in the above example, 15 or 16).

Telling piece (14,14) from (15,15) may be the major difficulty—we are to tell 0.13 from 0.09, with the existence of possible fluctuations.

Although it is not necessary to follow the above procedure, we do believe that the total output, peak/total, left/peak, right/peak ratios contain most of the information available. Their fluctuation and dependence on various parameters are studied.

5.3.2 Location Dependence

Figure 5.3 gives the source location dependence of light outputs. Light source is at center of crystal piece (1,1), (2,2)...or (32,32)--one of the diagonal pieces. Light guide thickness is again 4cm.

Figure 5.3(A) gives the total light output vs. source location. The curve is basically periodic. The total output is higher for close-to-PMT-center crystal pieces, and lower for close-to-PMT-edge crystal pieces. There is a strong edge effect—the total light output for source location (1,1) and (32,32) is significantly lower. We may discard the outermost crystal pieces and use only the center 30x30 of the 32x32 array. The raw contribution to energy resolution(FWHM) is estimated to be:

2.36 x Sigma / Mean = 16%.

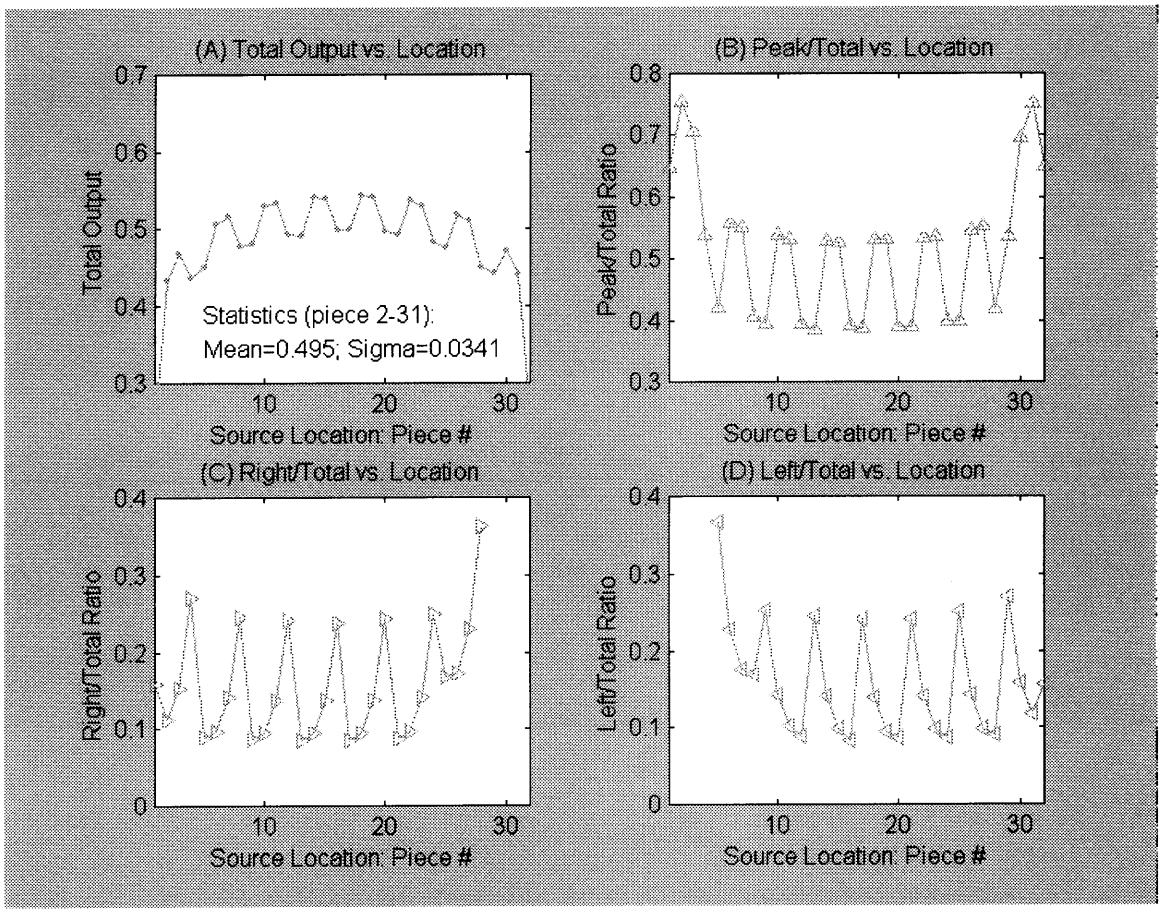

Figure 5.3: Source Location dependence of light output

When we sum the outputs of all PMTs, we also suffer from the fact that amplifying coefficients of different PMTs are not identical, and that the PMT response drifts.

These non-uniformities, however, could be partly eliminated with the method of calibration. The residue error is by practice within 3%, which means with no other source of broadening, the energy resolution is about 3%(FWHM).

Figure 5.3(B), (C), (D) give the Peak/Total, Right/Total, Left/Total ratios. They are also periodic for the same reason. The difference in the ratios is obvious. Of our most concern, the Left/Total(and Right/Total) ratios of the following groups can be steadily discriminated (2,2)&(3,3), (6,6)&(7,7), (10,10)&(11,11), (14,14)&(15,15), (18,18)&(19,19), (22,22)&(23,23), (26,26)&(27,27), (30,30)&(31,31). The two crystal pieces in each group sit at different sides of one PMT center, and are the most difficult to tell.

We conclude that a spatial resolution of 2.5cm is readily achievable, but more attention should be paid to the pieces close to edges.

5.3.3 Light Guide Thickness Dependence

Figure 5.4 shows the dependence of outputs on light guide thickness. Light source is at the center of corresponding crystal piece.

Figure 5.4(A) & 5.4(B): 1-D light output distributions for light source at crystal piece (15,15) or (16,16) respectively.

Figure 5.4(C): Total Light output as a function of light guide thickness.

Figure 5.4(D): Left/Total & Right/Total ratios as functions of light guide thickness.

When the light guide is only 1cm thick, the 1-D distributions are relatively sharply peaked, the difference between piece (15,15) total output and that of piece (16,16) is large (0.63 vs. 0.39), and the Left/Total and Right/Total ratios are almost the same for piece (15,15). These all mean insufficient light distributing.

As the light guide gets thicker, the total light output for pieces (15,15) and (16,16) gets closer. This means smaller location fluctuation and possibly better energy resolution after

calibration. Also with thicker light guide, the Left/Total and Right/Total ratios for piece (15,15) go apart, which enables us to tell piece (15,15) from piece (14,14). Please also refer to figure 5.2.

The optimal light guide thickness for an infinite crystal array is 5cm, as can be seen from figure 5.4(C) and (D). If we choose 4cm, however, it could be easier for us to handle pieces close to edges (those covered by PMT #1 or #8), because the 1-D distribution is more sharply peaked than in the 5cm thick light guide situation. From figure 5.4(B), we can see that for piece (16,16), the peak output is the same at 1 cm or 4cm light guide thickness.

A more sharply peaked 1-D distribution also means higher ability to discriminate multi-Compton events, which exist in our detector assembly. In these events there are two or more light sources, but we can not tell which is the original one.

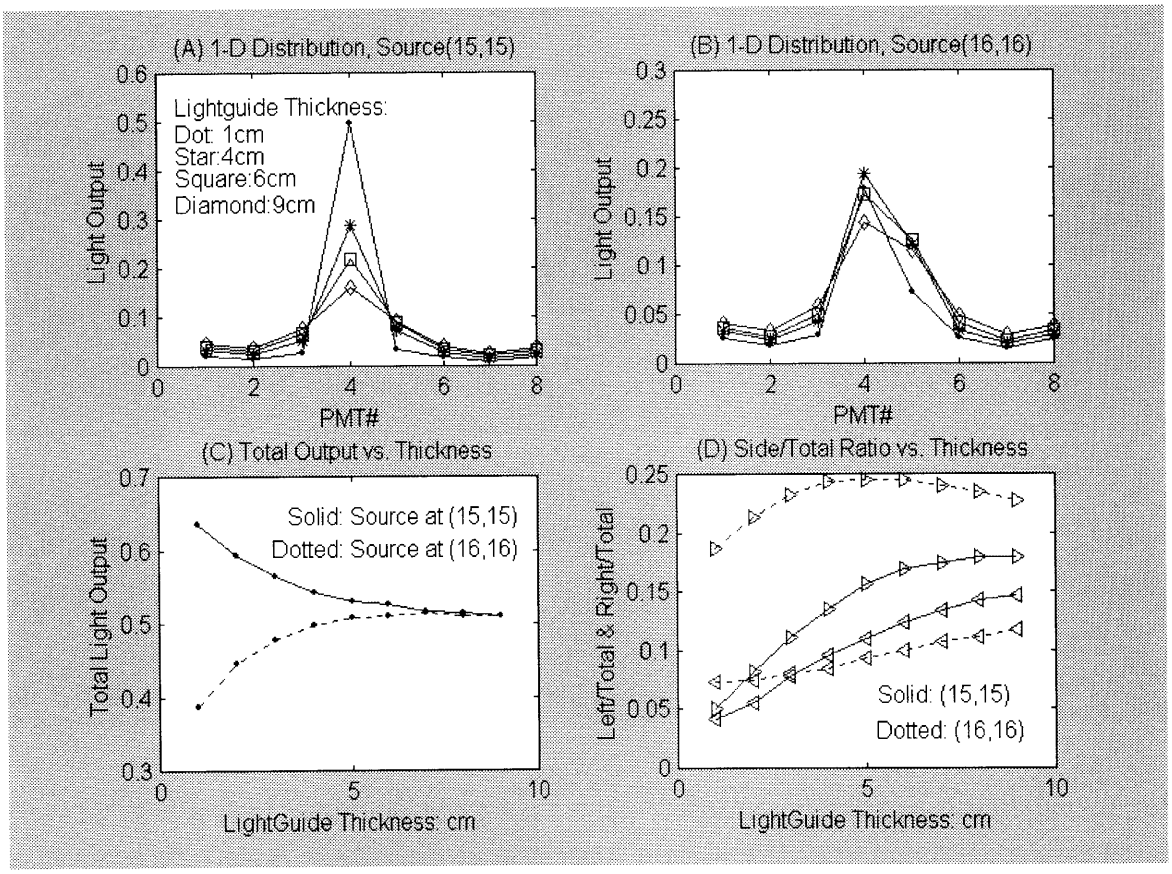

Figure 5.4: Light guide thickness dependence

5.3.4 Source Depth Dependence

Figure 5 shows the source depth dependence. This time the light source is on the central line of the crystal piece but the depth changes from 0cm to 10 cm. The light guide thickness is 4cm.

The 1-D distributions (figure 5.5 (A) and (B)), The total light outputs (figure 5.5(C)), and the Left/Total and Right/Total ratios (figure 5.5(D)) have very little dependence on light source depth. It is easy to understand. At whatever depth, if the scintillation photon goes toward the light guide(rear surface of crystal), it first attempts exiting the crystal. Otherwise if it goes toward the front surface, it first reaches the powder reflector. The scintillation photon has a 50% chance to go either way independent of the depth.

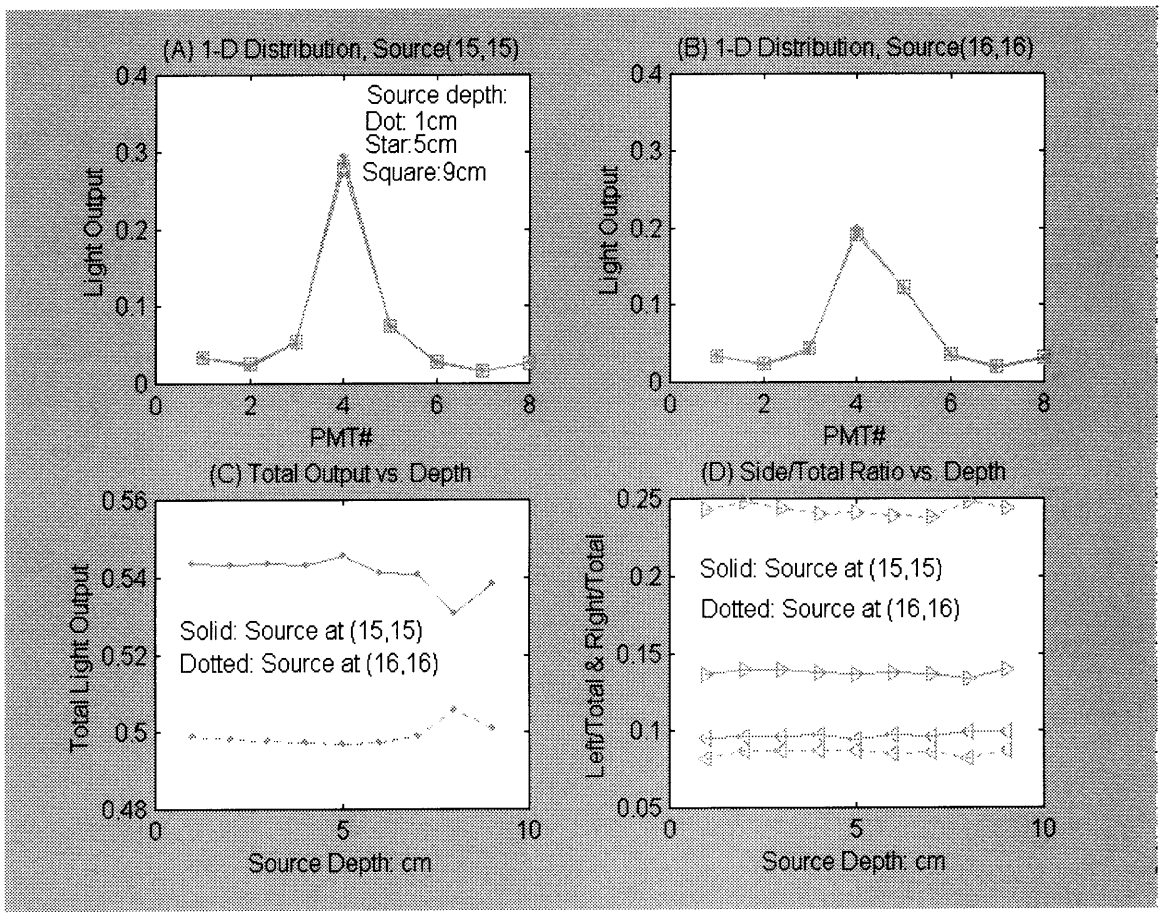

Figure 5.5: Source depth dependence (AIRGAP)

5.3.5 Evaluation

Air-Gap installation, with a 0.1mm thick air gap in between the polished crystal pieces, has very little source depth dependence of either total light output or 1-D output distribution. The optimal light guide thickness is determined to be 4cm.

The typical energy resolution of a 12.5cm cubic NaI(Tl) single detector at 6.13Mev is 4% (FWHM) [17]. The major additional contribution to energy resolution comes from the residue error of calibrating and compensating the location dependence and PMT response non-uniformity, which is previously declared to be 3% (FWHM) for 6.13Mev gamma ray. Thus the energy resolution of our detector assembly(not using the outermost crystal pieces) can be roughly estimated to be:

$$((3\%)^2 + (4\%)^2)^{1/2} = 5\% \text{ (FWHM)}.$$

This energy resolution is adequate for our use.

The 1-D distribution patterns are readily discernible, at different source location and depth. A spatial resolution of 2.5cm is achievable.

One major problem is the mechanical stress caused by the weight of crystal. We may wrap both ends of the crystal pieces with Teflon tape, forming an airgap between most part of the interface. The crystal pieces are supported on a small area at both ends. The total side surface area of a crystal piece is 2.5cmx10cm. If the area of contacting is 2.5cmx0.5cm at each end, the weight of the crystal assembly may cause a huge stress to the pieces at the bottom. The stress is about 3 times that caused by air pressure. This means a possible problem to the relatively soft NaI(Tl) crystal.

Another problem comes from the fact that NaI(Tl) is hydroscopic, which adds the requirement of sealing the whole assembly.

With the same amount of PMTs, the same method might work for more (and therefore smaller) crystal pieces. For example, each PMT covers a 5x5 crystal array, with each piece 2cm by 2cm. The difficulty is that the gamma ray of interested energy leads to a multi-scintillation event. There are at the same time two or more scintillation light sources.

If the original interaction of gamma ray with detector material is pair production, the kinetic energy of electron/positron pairs dominants the 1-D light output pattern. The energy deposited by the 0.511Mev annihilation photon(s) is not enough to influence our decoding procedure much. If a multi-Compton event occurs within one crystal piece, we just treat it as if it were a single scintillation. If the original interaction is Compton scattering, and the successive interactions occur at different crystal pieces, we do not have enough information to assign the gamma ray to a specific crystal piece. For example, the weighted sum of a (15,15) pattern and a (18,18) pattern may to some extend look like a (16,16) pattern. We need to identify and discard such multi-Compton events. If smaller (and more) crystal pieces are used, there are more patterns and the distinction among them go smaller. Generally speaking, if we cut the crystal into smaller pieces, we need more photo tubes.

The polished surface may not be absorption-free, as we assume in our model. Its effect becomes significant as the crystal pieces (bars) go thinner and thinner. 2.5cmx2.5cm cutting leads to a 4:1 ratio of axial dimension and cross-sectional dimensions. (Recall that our crystal is 10cm thick). This ratio is controlled below or about 4:1 in practice.

For gamma ray of about 5Mev energy in Sodium Iodide, the pair production cross section is about the same as that of Compton scattering. For 2.31Mev gamma ray, the pair production cross-section is significantly lower. We could choose to use 4.44Mev gamma ray for carbon, 5.10Mev Gamma ray for nitrogen, and 6.13Mev gamma ray for oxygen. Pair production events are to be recorded and multi-Compton events are to be discarded.

5.4 Comparison with Other Designs

5.4.1 Diffuse Interface

We may make the crystal surfaces rough by sanding them, and fit them together tightly so that there is no macroscopic airgap. Ideally the resulting interface is an isotropic diffuser. This is the Diffuse Interface Installation. Again light is collimated and distributed

simultaneously. The optimal light guide thickness is 0.75cm and the location dependence of light output is similar.

Figure 5.6 shows the source depth dependence of light outputs for Diffuse Interface Installation. Several differences are as follows:

The total light output strongly depends on light source depth. This means a poor energy resolution.

The Left/Total and Right/Total ratios for crystal piece (15,15) both decrease with the source depth increasing, but the difference between the two ratios remains. The spatial decoding procedure described above still works.

The 1-D distribution patterns are simpler. Light output is highly concentrated on the three PMTs close to the light source, and there is virtually no light output from other PMTs. This is good for identifying multi-Compton events.

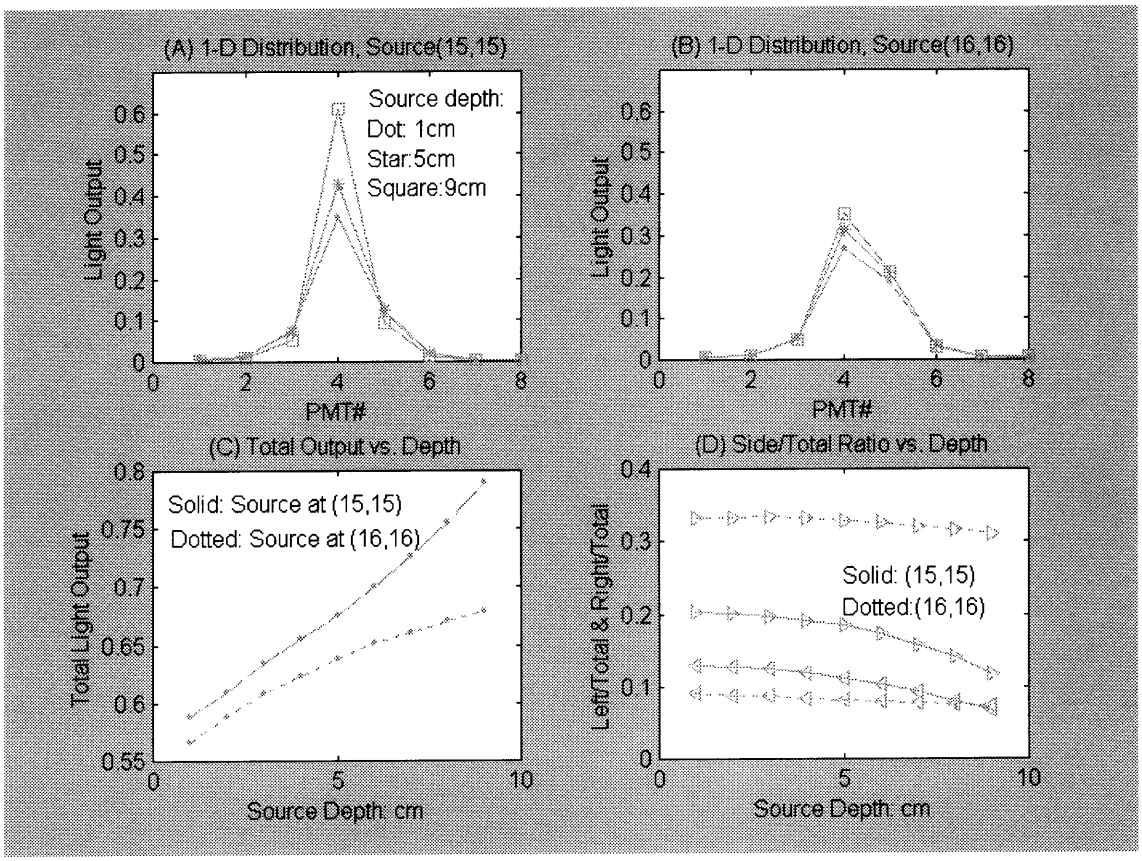

Figure 5.6: Source depth dependence (DIFFUSE)

Before reaching the light guide (or the rear surface) and attempting to exit, light at a small depth has more chance to reach the powder reflector at the front surface. Because the powder reflector absorbs light, the total light output varies with light source depth. The resulting poor energy resolution makes the installation acceptable in our system.

In the Diffuse Interface Installation, light is isotropically diffused each time it reaches the crystal piece interfaces. Once light is close to the light guide, it is easier to pass the unmatched crystal-light guide interface. The overall distributing effect is less than that in the Multi-layer situation. And the 1-D distribution pattern is more sharply peaked.

5.4.2 Reflective Interface

Reflective Interface is to apply a layer of powder reflector between polished crystal pieces. Generally a thick light guide is needed in this installation. Light is collimated by the optimally isolated crystal pieces, and then distributed in the light guide. This in concept is similar as the PET detectors. Here we don't count for the energy loss of fast electron in reflector material.

The optimal light guide thickness is 18cm for Reflective Interface Installation. The should not be a surprise, however, because light is collimated by the crystal pieces into a narrow cone region and need to be distributed to at least 3 PMTs(Each PMT covers a 10cm region).

Figure 5.7 shows the light source depth dependence of light outputs.

Light in the present installation experiences powder reflection at the crystal piece interfaces, and therefore the total light output is by far less than in the Diffuse Interface Installation. Other features are also poorer than in the Diffuse Interface Installation.

We may get an insight of improving the PET detector. If we replace the Reflective interface with Diffuse interface, we not only save the cost of the BGO light guide, but also obtain higher light output, better energy resolution and most importantly, possible higher crystal piece/PMT ratio. Recall that one PMT is possible to decode more than a 4x4 crystal array, if we are dealing with single scintillation events.

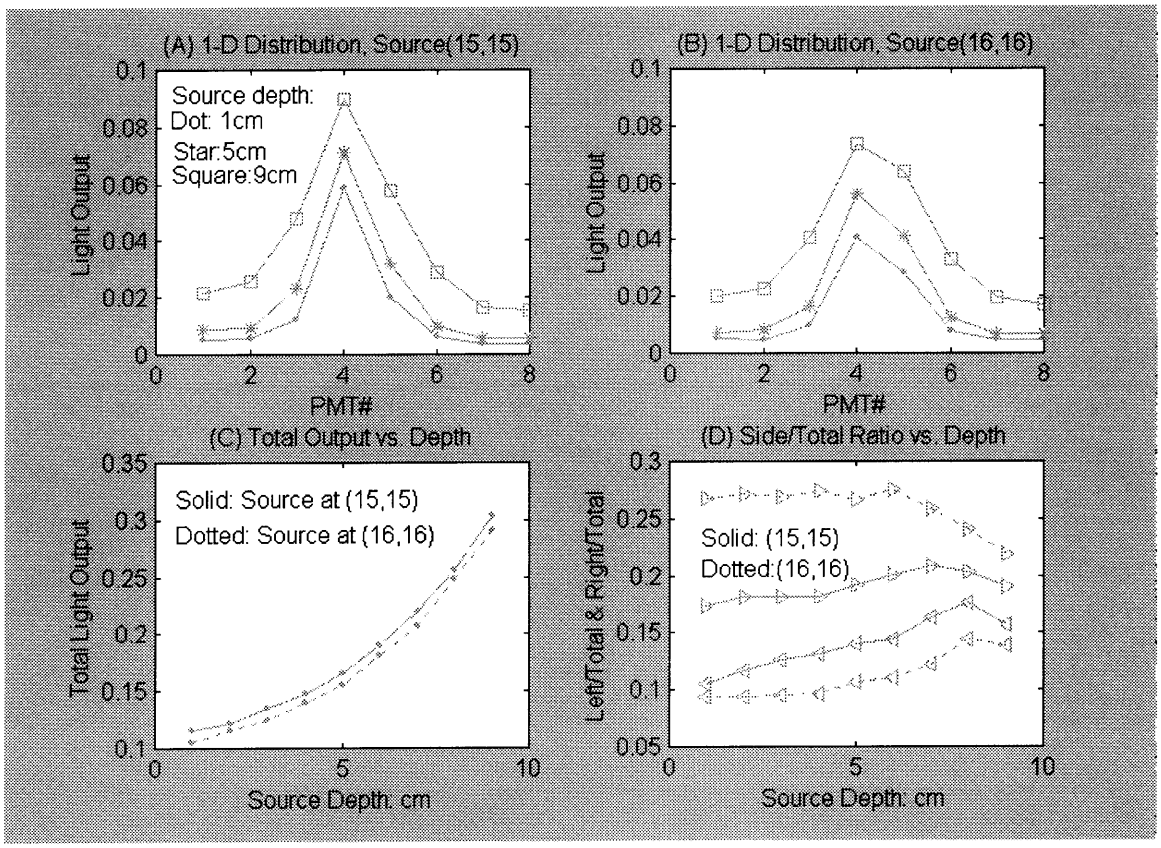

Figure 5.7: Source depth dependence (REFLECTIVE)

5.4.3 Single Crystal

At last we give the simulation result for Single Crystal Installation. here a single large crystal is used and a 0.75cm thick Pyrex light guide is attached. In this installation, scintillation light is not collimated.

Figure 5.8 gives the source depth dependence of light outputs. It is not possible to achieve a 2.5cm spatial resolution with our method, even for single scintillation events. If we locate the scintillation events to a continuous distribution, as it is in Anger Camera, the FWHM of spatial resolution would be larger than 1cm and cell width of more than 2.5cm is to be used [20]. Another disadvantage of Single Crystal Installation is that the usable area is only a small part at center. Single Crystal design works only when the crystal is relatively thin.

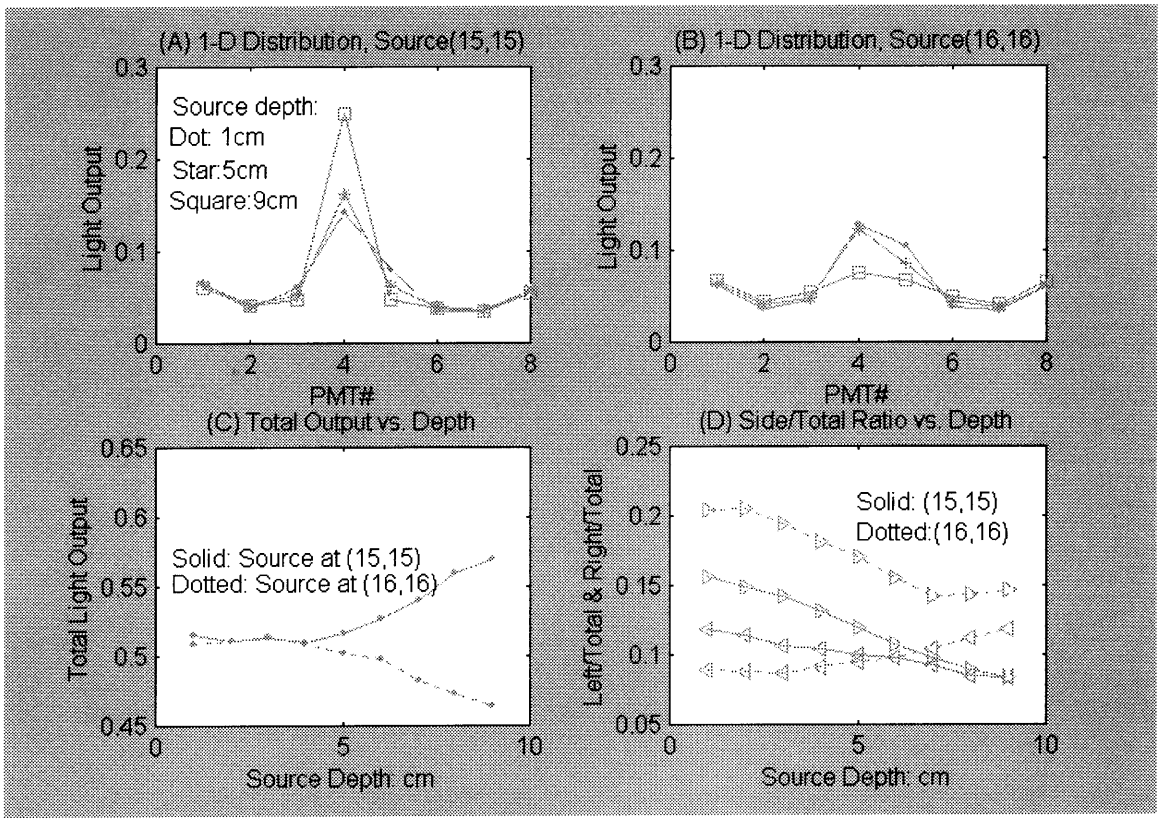

Figure 5.8: Source depth dependence: (SINGLE)

Chapter 6 BGO Detector Design

An alternative choice of detector material is BGO. Compared with NaI(Tl), BGO has both higher atomic number (Z) and higher density. Thus it has much higher detection efficiency, as shown in chapter 4.

The drawbacks of BGO are its lower scintillation efficiency and higher refractive index (n). These lead to lower light output for given energy of electron (positron), which means poorer energy resolution in general.

In this chapter, we study by simulation the performance of a BGO bar detector. Its size is 20cm long by 8cm wide by 5cm thick. This is NOT directly useable for our CAFNA, but the method and results are the same for a longer bar detector (1-D detector), or a larger area detector (2-D detector).

6.1 Description

6.1.1 Assembly Arrangement

The BGO crystal is a 20cmx8cmx5cm bar. Because of the high refractive index (n=2.15 at its emission maximum) and therefore sever internal reflection, BGO does not work in the block arrangement introduced in last chapter.

In PET, slots are cut on the BGO crystal to a certain depth and reflective white powder is applied in the slots. [14] Light is isolated between the blocks but not between any block and the light guide. Light is collimated in the slotted blocks and distributed in the uncut layer, or the light guide, which is the same material. As we mentioned before, this kind of treatment leads to poor energy resolution, which is less a problem in PET.

If we leave an air gap between completely cut blocks, like the design in Chapter 5, the resulting assembly has insufficient light distribution, making it impossible to locate the events to an accuracy smaller than PMT size.

Fortunately, the thickness needed for acceptable detection efficiency is less for BGO. From the data in chapter 4, it's clear that 5cm thick large area BGO detector has a detection efficiency of about 45%, which is pretty promising. At this thickness, a single piece crystal gives a spatial resolution of 5-8mm. Anger camera [10] uses a single piece crystal. To improve the light output, we put PMTs at four sides as well as the rear surface.

A sketch is given in figure 6.1. Ten 3.8cm (1.5") PMTs are used at rear surface, five at top and five at bottom, also two at left and two at right. The front surface, which is inside the paper, is the gamma ray incident surface. All PMTs are equally spaced. The first row of PMTs are denoted as (2,1) through (6,1), second row as (1,2) through (7,2), third row as (1,3) through (7,3), and the fourth row as (2,4) through (6,4). There are altogether 24 PMTs.

No light guide is applied, but white powder reflector is applied on front surface and gaps on other surfaces.

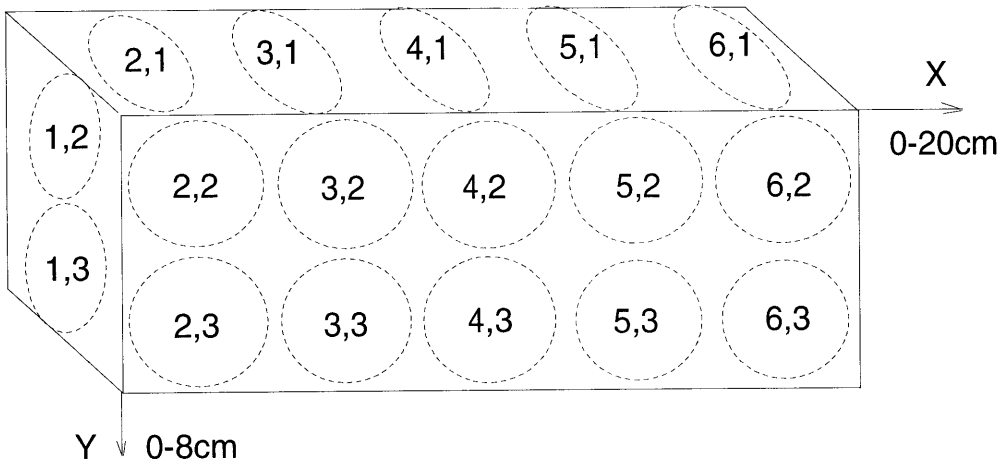

Figure 6.1 BGO detector

6.1.2 Modeling

In the simulation of light propagation, the following facts are assumed.

- Each scintillation event is represented by a point light source, located on the central line of a crystal piece. If no source depth is specified, the source is at the center of that crystal piece. This is not quite accurate because fast electrons/positrons may travel several millimeters in BGO.
- 10,000 photons are computed for each scintillation event. Typically a 1.2Mev gamma ray gives that amount of light in BGO[12][13]. These photons spread out isotropically.
- BGO crystal absorbs the scintillation light, and the absorption length is taken as 400mm [16].
- All photons are assigned a wavelength of 505nm, the emission maximum.
- The refractive indexes are taken as: BGO:2.15; Glass (PMT Window):1.5
- The average reflectivity of white reflector is taken as 97%. This is practical with titanium dioxide or magnesium oxide reflective powder, for the emission spectrum of BGO (maximum wavelength 505nm)[12][13].
- At PMT windows, light undergoes either internal reflection or Fresnel reflection/refraction. Polarization is NOT considered.
- At Reflective surfaces, which are coated with powder reflector, photons are either absorbed (with a probability of 3%) or scattered back isotropically.

6.2 Energy Resolution

Energy resolution is mainly determined by the fluctuation of total light output. Scintillation events at different location or depth lead to different amount of photons (visible light) exiting from crystal to PMTs.

6.2.1 Location Dependence

Figure 6.2 shows the location dependence of total light output. The total light output at the center part of 1-19cm (x-direction) and 1-7cm (Y-direction) is 0.62±0.014.

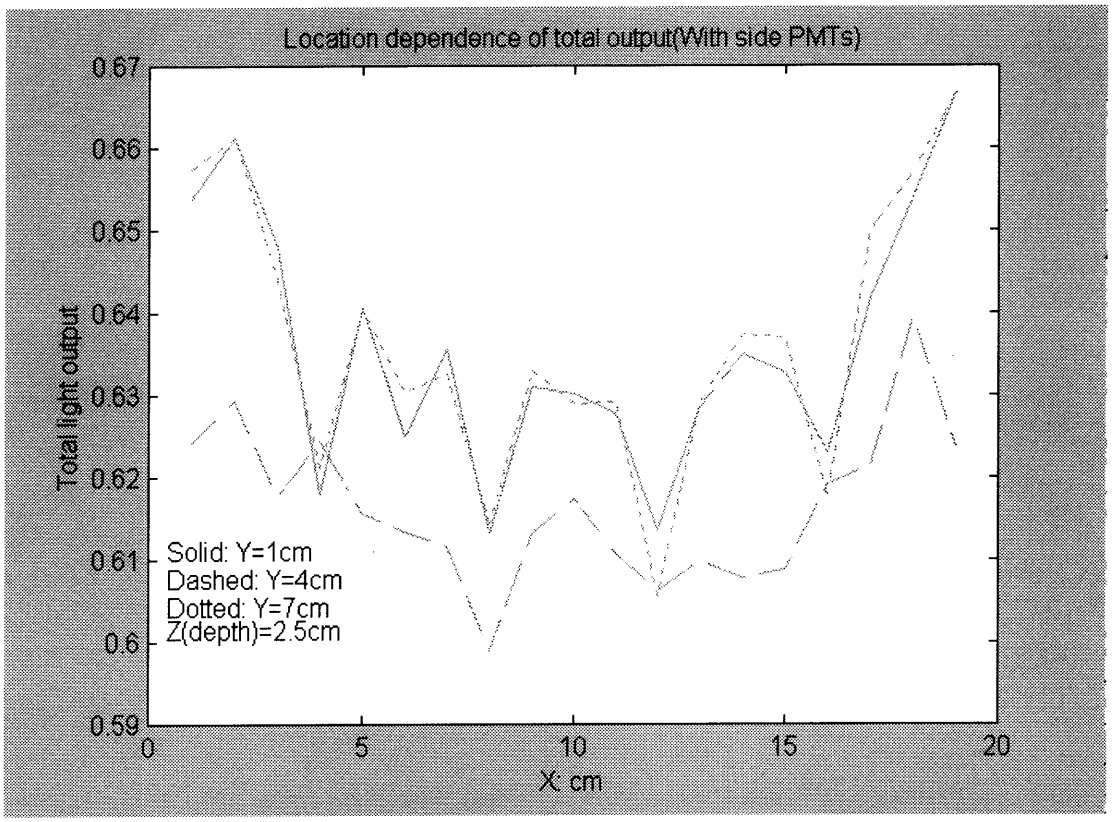

Figure 6.2 Location dependence of total light output

6.2.2 Depth Dependence

Figure 6.3 shows the depth dependence of total light output. Total light output at center part (Again only a 1cm edge is excluded) is 0.62±0.011.

It's clear that with the PMTs at side surfaces, the light output is comparable with NaI(Tl).

Without any post calibration, the energy resolution FWHM can be estimated as:

$$2.355 \times (0.014^2 + 0.011^2)^{1/2} / 0.62 = 7\%.$$

At our gamma ray energy, the contribution of statistics is minor.

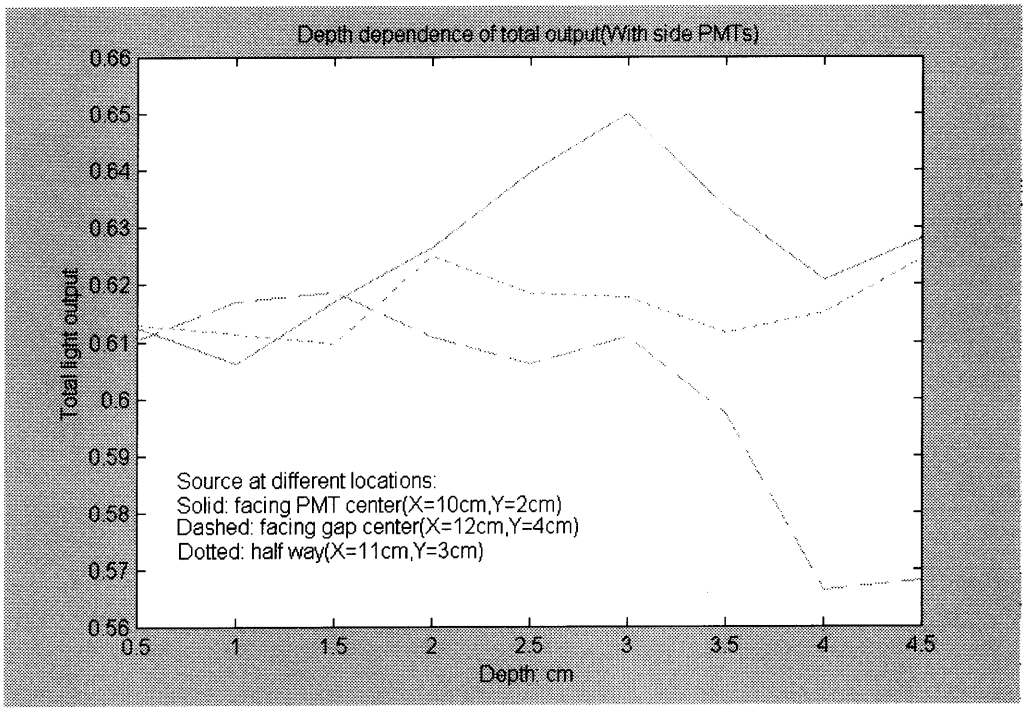

Figure 6.3 Depth dependence of total light output

6.3 Spatial Resolution

Because of the light spread, spatial resolution of 5cm thick crystal is 5-8mm [10][18]. This has been testified in the practice of Anger camera. The coordinates are calculated with the outputs of PMTs. As we mentioned previously, light propagation in X and Y direction is independent with each other. Therefore the two coordinates are calculated independently.

Generally, the X-coordinate is calculated through the equation:

$$X = \sum_i Ci * \sum_j COUNT(i, j)$$

Where C_i is the calibration coefficient for i^{th} column PMTs, and COUNT(i, j) is the output of number (i, j) PMT. C_i is determined experimentally in advance. The same equation stands for Y.

Listed below is a piece of simulated data of light distribution. Total number of photons (scintillation light) is 10,000. Each number behind COUNTX in the list is the sum of corresponding column of PMTs' outputs.

Y= 1 cm; Z=1-5cm, exponential distribution.

X= 1cm; COUNTX: 1614 3477 596 237 188 181 395
X= 2cm; COUNTX: 1413 3423 636 293 178 207 428
X= 3cm; COUNTX: 1222 3222 863 329 187 217 451
X= 4cm; COUNTX: 1046 1992 1635 431 214 254 505
X= 5cm; COUNTX: 964 1081 2825 473 244 275 532
X= 6cm; COUNTX: 851 821 3048 554 254 264 543
X= 7cm; COUNTX: 890 695 2777 767 302 303 573
X= 8cm; COUNTX: 800 595 1661 1596 441 380 667
X= 9cm; COUNTX: 739 500 774 2773 508 360 680
X=10cm; COUNTX: 682 406 517 2971 601 410 696
X=11cm; COUNTX: 709 377 499 2829 771 432 759
X=12cm; COUNTX: 661 325 436 1573 1638 645 839
X=13cm; COUNTX: 531 287 304 818 2880 701 816
X=14cm; COUNTX: 555 302 239 519 2986 817 898
X=15cm; COUNTX: 547 279 214 487 2835 1038 987
X=16cm; COUNTX: 525 248 248 409 1647 2024 1107
X=17cm; COUNTX: 427 208 188 305 850 3234 1189
X=18cm; COUNTX: 488 173 175 299 649 3413 1440
X=19cm; COUNTX: 416 198 158 251 632 3373 1563

One can easily tell the rule of number changing in the list. The list is the input of the equation above. Here we don't guess how well we can do—The spatial resolution in this situation is better to be studied experimentally. Practice of Anger camera suggests 5-8mm spatial resolution.

Chapter 7 Summary

7.1 Conclusions

Coded Aperture Imaging Fast Neutron Analysis is a promising technique for explosive and drug inspection. It is also good for other situations where elemental mapping is needed.

In this thesis we have shown that:

- Explosives and drugs have distinctive element contents for FNA.
- Fast neutron (and also thermal neutrons) induces prompt gamma ray of different energy from different elements.
- 14Mev neutron has adequate penetrating power to be practical.
- Coded Aperture Imaging offers the reconstructed image from collected data.
- The imaging detector to be used must have reasonable energy resolution, spatial resolution and detection efficiency.
- A NaI(Tl) detector assembly is proposed for direct use.
- A small BGO bar detector is studied for the purpose of building one of practical size.

7.2 Future Work

To demonstrate the technique of Coded Aperture Imaging Fast Neutron Analysis and its application in contraband inspection, we are moving to the experimental stage. Major activities are:

- Determination of the optimal spacing of neutron source, object, coding mask, and detector.

- Radiation protection design.
- Coded Aperture Imaging algorithm.
- Calibrate the detector for locating process.
- Spectral analysis. Useful information is not only carried by the full energy peaks of a recorded pulse-height spectrum.

Appendix Source Code for NaI simulation

The following is the source codes of NaI light propagation simulation.

The first part is the main program, which simulates the depth dependence. Function *sample* tracks the whole process of a scintillation photon.

```
#include <stdio.h>
#include <math.h>
#include <string.h>
#include "nai.h"

/*This program calls function sample in the head file nai.h.*/

/*Input parameters:*/
/*no[0] contains X-number of the NaI piece in which scintillation occurs*/
/*no[1] contains Y-number of the NaI piece in which scintillation occurs*/
/*no[2] holds nothing when used as input*/
/*Depth of the scintillation spot and light guide thickness are also input*/

/*Output parameters:*/
/*no[0] returns X-number of the PMT where the photon exits*/
/*no[1] returns Y-number of the PMT where the photon exits*/
/*no[2] returns the collision numbers of the photon.*/
/*function sample itself returns 1 if photon exits or 0 if photon is absobed*/

main()
{int no[3], record, count[8][8], countx[8], lost, piece, i, j;
 long int colls;
 double thick=4.0;
 srandom(time(0)*getpid());
```

```
for (depth=1;depth<10; depth+=1)
  {  lost=0;colls=0;
     for (i=0;i<8;i++)   countx[i]=0;
     for (j=0;j<100000;j++)
       { no[0]=15;no[1]=15; no[2]=0;
            if(!sample(&(no[0]), depth, thick)) lost++;
            else  countx[no[0]]++;
         colls+=no[2];
       }
     colls/=100000;
     printf("%4.2f  ", depth);
     printf("%5d ", 100000-lost);fflush(stdout);
     for (i=0;i<8;i++) printf("%5d ",countx[i]);
     printf("%4d", colls);
     printf("\n");
   }
}
```

The second part is the head file, which offers basic functions, including *sample*.

```
#include<math.h>
#include<stdio.h>
#include<string.h>
#define NCRY  32   /*NCRY by NCRY pieces of crystals*/
#define NPMT  8    /*NPMT by NPMT pmts*/
#define SIZE  80.0   /*total area is SIZE by SIZE*/
#define REFL  0.9  /*Powder Reflectivity*/
#define NNAI  1.85 /*Refractive Index of NaI*/
#define NGLASS 1.5 /*Reflective Index of glass*/

void isotrop(double *direct)   /*Generates an isotropic distribution*/
  {double u,v,w,phi;
```

```
  u=((double) random())/((double) 0x7fffffff);
  u=2*u-1;
  phi=((double) random())/((double) 0x7fffffff);
  phi=phi*2*3.1415926;
  v=sqrt(1-u*u); w=v;
  v=v*cos(phi); w=w*sin(phi);
  *direct=u;
  *(direct+1)=v;
  *(direct+2)=w;
 }

int diffuse(double *direct, int normal, int type)
  /*diffuse boudary performance*/
  /*input old direction cosines by address direct*/
  /*input normal of surface: 0-5: x-,x+,y-,y+,z-,z+*/
  /*input type of surface: 0--partial reflection; 1--ISO diffuse*/
  /*return new direction cosines in direct*/
  /*return 0 if absorbed; 1 if not*/
  {int axis, i;
  double od,nd[3]={0,0,0};
  switch (normal)
    { case 0: case 1: axis=0;break;
      case 2: case 3: axis=1;break;
      case 4: case 5: axis=2;break;
    }
  od=*(direct+axis);
  while (nd[axis]==0) isotrop(&(nd[0]));
  if (type==0)
    { if (((double) random())/((double) 0x7fffffff)<1-REFL) return(0);
      while ((nd[axis])*od>=0) isotrop(&(nd[0]));
    }
  for (i=0;i<3;i++) *(direct+i)=nd[i];
  return(1);
```

```
}

void fresnel(double n1, double n2, double *direct)
  /*fresnel reflection/infraction*/
  /*input indexes n1, n2*/
  /*input cosine of incident angle*/
  /*output cosine of outgoing angle*/
  {double sin1,sin2,cos1,cos2,rp,rs;
  cos1=*(direct+2);
  sin1=sqrt(1-cos1*cos1);
  sin2=n1*sin1/n2;
  cos2=sqrt(1-sin2*sin2);
  if (cos1<0) cos2*=-1;
  rp=(n2*cos1-n1*cos2)/(n2*cos1+n1*cos2);
  rs=(n1*cos1-n2*cos2)/(n1*cos1+n2*cos2);
  rp=0.5*(rp*rp+rs*rs);
  if (rp>((double) random())/((double)0x7fffffff))
    *(direct+2)=-1*cos1;
  else { (*direct)*=sin2/sin1;
       (*(direct+1))*=sin2/sin1;
           *(direct+2)=cos2;}
  }

void gapfresnel(double n1, double *direct, int axis)
  /*Airgap fresnel reflection/infraction*/
  /*input indexes n1, the other is 1.0*/
  /*input cosine of incident angle*/
  /*output cosine of outgoing angle*/
  {double sin1,sin2,cos1,cos2,rp,rs,n2=1.0;
  cos1=*(direct+axis);
  sin1=sqrt(1-cos1*cos1);
  sin2=n1*sin1/n2;
  cos2=sqrt(1-sin2*sin2);
```

```
  if (cos1<0) cos2*=-1;
  rp=(n2*cos1-n1*cos2)/(n2*cos1+n1*cos2);
  rs=(n1*cos1-n2*cos2)/(n1*cos1+n2*cos2);
  rp=rp*rp; rs=rs*rs;
  rp=rp*(2-rp); rs=rs*(2-rs);
  rp=0.5*(rp+rs);
  if (rp>((double) random())/((double)0x7fffffff))
     *(direct+axis)=-1*cos1;
  }

void spectacular(double *direct, int axis)
  /*performance in spectacular surface*/
  /*input incident direction cosine*/
  /*return outgoing direction cosine*/
  /*w>0 means from crystal to light guide,*/
  /*where internal reflection is possible*/
  { axis= (int) axis/2;
    if (axis==2)
      {if (*(direct+2)<0) fresnel(NGLASS,NNAI,direct);
       else { if(*(direct+2)>sqrt(1-NGLASS*NGLASS/(NNAI*NNAI)))
              fresnel(NNAI,NGLASS,direct);
             else (*(direct+2))*=-1;
             }
      }
     else
      {if ((*(direct+axis))*(*(direct+axis))<1.0-1.0/(NNAI*NNAI))
         (*(direct+axis))*=-1;
       else gapfresnel(NNAI, direct, axis);
      }
  }

 int travel(double *locat, double *direct, double *bound)
   /*travel in a rectangular cube, */
```

```
 /*which extents from(0,0,0) to positive XYZ*/
 /*input original relative location in locat*/
 /*input original direction cosines in direct*/
 /*input upper boundary of X,Y,Z in bound*/
 /*return new location at locat*/
 /*return id of final surface: 0-5:x-,x+,y-,y+,z-,z+*/
{double l[3],b[3],d[3],r[3];
 int normal=0;
 int i;
 for(i=0;i<3; i++)
   {l[i]=*(locat+i);
    d[i]=*(direct+i);
    b[i]=*(bound+i);
    if(d[i]>0) r[i]=(b[i]-l[i])/d[i];
    else if (d[i]==0) r[i]=10000;
        else  r[i]=-1*(l[i]/d[i]);}
 for(i=0;i<3;i++)
   if (r[i]<r[normal]) normal=i;
 for(i=0;i<3;i++)
   *(locat+i)=l[i]+(r[normal])*(d[i]);
 if (d[normal]>0)
   { *(locat+normal)=b[normal]; return(normal*2+1);}
 else {*(locat+normal)=0; return(normal*2); }
}

int exitwindow(int *pmt, double *locat)
 /*process of end window*/
 /*input location at locat, only X&Y are used*/
 /*if exits to one of PMTs, return its # at pmt*/
 /*return 0 if exits, else return 1*/
 {int i,j;
  double x,y;
  for (i=0;i<NPMT;i++)
```

```
  for (j=0;j<NPMT;j++)
     {x=10*i+5-(*locat);
      y=10*j+5-(*(locat+1));
      if((x*x+y*y)<3.8*3.8)
         {*pmt=i;
          *(pmt+1)=j;
          return(0);}}
  return(1);
  }

void exchange(int *no, double w, double *locat)
     /*input traveling direction in w */
     /*input/output crystal piece # in no */
     /*if exits to one of PMTs, return its # at pmt */
     /*return 0 if exits, else return 1 */
  { if (w>0)
      { (*locat)+=2.5*(*no);
        (*(locat+1))+=2.5*(*(no+1));
        (*(locat+2))=0;}
    else
      {*no=(int) (*locat)/2.5;
       *(no+1)=(int) (*(locat+1))/2.5;
       (*locat)-=2.5*(*no);
       (*(locat+1))-=2.5*(*(no+1));
       (*(locat+2))=10;}
  }

 void intchange(int normal, int *no, double *locat, double *direct)
    /* interchange between crystal pieces */
  {switch (normal)
    { case 0: if (*(direct)<0)
              { (*(no))--; *(locat)=2.5;}
              break;
```

```
    case 1: if (*(direct)>0)
                { (*(no))++; *(locat)=0;}
            break;
    case 2: if (*(direct+1)<0)
            {(*(no+1))--; *(locat+1)=2.5;}
            break;
    case 3: if (*(direct+1)>0)
            {(*(no+1))++; *(locat+1)=0;}
            break;
    case 4: case 5: break;
  }}

int diffusetype(int *no, int normal)
   /* calculates diffuse type in crystal pieces */
   /*input piece id and surface id */
   /*return type: 0-93%reflection, 1-other*/
  {if (normal==4) return(0);
   if ((*no==0) && normal==0) return(0);
   if ((*no==(NCRY-1)) && normal==1) return(0);
   if ((*(no+1)==0) && normal==2) return(0);
   if ((*(no+1)==(NCRY-1)) && normal==3) return(0);
   return(1);
  }

 int sample(int *no, double depth, double thick)
    /* samples a photon */
    /* starts at depth of center line of #no piece */
    /* no input: crystal #x & #y, 0 */
    /* no output: pmt #x &#y, and if recorded, collissions */
    /*return 0 if lost, 1 if recorded */
  {double locat[3]={1.25,1.25, depth};
   double boundcry[3]={2.5,2.5,10};
   double boundguid[3]={SIZE,SIZE, thick};
```

```
 double direct[3];
 int normal, type, i,j;

 if (*no<0 || *no>=NCRY || *(no+1)<0 || *(no+1)>=NCRY) return(0);
 if (depth<0 || depth>10) return(0);

 *(no+2)=0;    /* sets colls to zero */
 isotrop(&(direct[0]));

cycle1:
 normal=travel(&(locat[0]), &(direct[0]), &(boundcry[0]));
/*
printf("Travels in piece %d %d, to surface %d ", *(no), *(no+1), normal);
printf("Direction:  %6.4f  %6.4f  %6.4f  Location:  %6.4f  %6.4f  %6.4f\n",  direct[0],
direct[1], direct[2], locat[0], locat[1],locat[2]);
*/
 if (normal==5)
   {spectacular(&(direct[0]),normal);
    (*(no+2))++;
    if (*(no+2)>500) return(0);
    if (direct[2]>0)
      {exchange(no, direct[2], &(locat[0]));
/*
printf("Enters lightguid.              Direction: %6.4f %6.4f %6.4f Location: %6.4f %6.4f
%6.4f\n",direct[0], direct[1],direct[2],locat[0],locat[1],locat[2]);
*/
      goto cycle2;}
    else goto cycle1;
   }
 else
   {type=diffusetype(no, normal);
    if (type)  spectacular(&(direct[0]),normal);
    else  if (!(diffuse(&(direct[0]), normal, type)))
```

```
        { (*(no+2))++; return(0);}
    (*(no+2))++;
    if ((*(no+2))>500) return(0);
/*
printf("Diffuse: type %d, surface: %d                newdirect: %6.4f %6.4f %6.4f\n",
type,normal, direct[0],direct[1],direct[2]);
*/
    intchange(normal, no, &(locat[0]), &(direct[0]));
/*
printf("Enters piece %d %d,                Direction: %6.4f %6.4f %6.4f Location: %6.4f
%6.4f %6.4f\n", *(no), *(no+1),direct[0], direct[1],direct[2],locat[0],locat[1],locat[2]);
*/
    goto cycle1;
   }


 cycle2:
  normal=travel(&(locat[0]), &(direct[0]), &(boundguid[0]));
/*
printf("Travels in lightguid, to surface %d ", normal);
printf("Direction: %6.4f %6.4f %6.4f Location: %6.4f %6.4f %6.4f\n", direct[0],
direct[1], direct[2], locat[0], locat[1],locat[2]);
*/


  if (normal==4)
   { spectacular(&(direct[0]),normal);
    (*(no+2))++;
    if ((*(no+2))>500) return(0);
    if (direct[2]<0)
        {exchange(no, direct[2], &(locat[0]));
/*
printf("Enters piece %d %d, ", *no,*(no+1));
printf("                Direction: %6.4f %6.4f %6.4f Location: %6.4f %6.4f %6.4f\n",
direct[0], direct[1], direct[2], locat[0], locat[1],locat[2]);
*/
```

```
          goto cycle1;}
     else goto cycle2;
    }
  if (normal==5)
     if (!exitwindow(no, &(locat[0])))
        {
/*
printf("Recorded: PMT %d %d\n", *no,*(no+1));
*/
          return(1);
        }
  if (diffuse(&(direct[0]), normal,0))
    { (*(no+2))++;
      if ((*(no+2))>500) return(0);
      goto cycle2;
    }
  else { (*(no+2))++; return(0);}
  }
```

References

[1] S. M. Khan, editor. *Proceedings of the First International Symposium on Explosive Detection Technology*, New Jersey, November, 1991. Federal Aviation Administration, US Department of Transportation, FAA Technical Center.

[2] Tsahi Gozani, Advances in Accelerator-Based Explosives Detection Systems. *NIM(B),* No. 79 (1993), PP. 601-604.

[3] O. Serra: *Developments In Petroleum Science 15A: Fundamentals of Well-Log Interpretation*, Elsevier, 1984.

[4] R. C. Hertzog et al: "Neutron-excited Gamma-ray Spectrometry for well logging", *IEEE Transactions on Nuclear Science*, Vol. NS-26, No. 1, 1979.

[5] H. E. Hall and T. W. Bonner: "Gamma Radiation from Inelastic Scattering of Fast Neutrons in C^{12}, N^{14}, and O^{16}", *Nuclear Physics* 14 (1959/1960), PP.295-313.

[6] J. L. Perkin: "Gamma Ray Spectra from fast Neutron Interactions", *Nuclear Physics*, 60 (1964), PP. 561-580.

[7] Nuclear Database. *http://t2.lanl.gov*. Los Alamos National Laboratory.

[8] H. H. Barrett and W. Swindell. *Radiological Imaging*, Volume 1&2. Academic Press, New York, 1981.

[9] L. Mertz and N. O. Young. "Fresnel Transformation of Images (Fresnel Coding and Decoding Images). " *Proceedings of the Conference on Optical Instruments and Techniques*, PP.305-312, London, 1962.

[10] Anger H. O. 1958, Rev. Sci. Instrum. 29 pp.27-33.

[11] Li Zhang, *Coded Aperture Imaging for Fast Neutron Activation Analysis*. Master of Science Thesis, 1992, MIT-NED.

[12] Glenn F. Knoll. *Radiation Detection and Measurement*. John Wiley & Sons, 1989.

[13] Birks J.B., *The Theory and Practice of Scintillation Counting*, Pergamon Press, 1964.

[14] M.E. Casey and R. Nutt, "A Multicrystal Two Dimensional BGO Detector System For Positron Emission Tomography", *IEEE Transactions on Nuclear Science*, Vol.33, No.1, February 1986.

[15] Stephen E. Derenzo and John K. Riles, "Monte Carlo Calculations of The Optical Coupling Between Bismuth Germanate and Photomultiplier Tubes", *IEEE Transactions on Nuclear Science*, Vol. NS-29, No.1, February 1982.

[16] BICRON *Products Brochure*, Saint-Gobain/North Industrial Ceramics Corporation.

[17] Horst Scholermann and Horst Klein: "Optimizing the Energy Resolution of Scintillation Counters at High Energies", *NIM* 169 (1980), PP.25-31.

[18] S. Surti et al: "Slotted Surface Treatment on Position-Sensitive NaI(Tl) Detectors to Improve Spatial Resolution", *Proceedings of 1997 IEEE Nuclear Science Symposium.*

[19] Changsong Ji: *Handbook of Nuclear Radiation Detectors and Their Experiment Techniques*, Atomic Press (China), 1990.

[20] W. R. Cook, M. Finger, and T. A. Prince, "A Thick Anger Camera for Gamma Ray Astronomy", *IEEE Transactions on Nuclear Science.*